Optical response of alternating twisted trilayer graphene

Dionisios Margetis [1,*] Guillermo Gómez-Santos,[2,†] and Tobias Stauber [3,‡]

[1]*Department of Mathematics, and Institute for Physical Science and Technology, University of Maryland, College Park, Maryland 20742, USA*
[2]*Departamento de Física de la Materia Condensada, Instituto Nicolás Cabrera and Condensed Matter Physics Center (IFIMAC),*
Universidad Autónoma de Madrid, E-28049 Madrid, Spain
[3]*Instituto de Ciencia de Materiales de Madrid, CSIC, E-28049 Madrid, Spain*

We study the optical response of the alternating twisted trilayer graphene by making use of a unitary transformation for the trilayer Hamiltonian and the Kubo formulation of linear response theory. The layer-resolved optical conductivities are expressed in terms of contributions from *effective* twisted bilayer and single-layer systems along with their coupling. We show that the in-plane magnetic response is proportional to this coupling between the twisted bilayer and single-layer systems; and, due to the different energy scales, the in-plane magnetic response is negligibly small. We also formulate a *local* electromagnetic response that involves the vertical gradients of the magnetic field and moment.

I. INTRODUCTION

In 2018, it was shown that the twist angle between two graphene layers can be tuned so that correlated insulator phases [1] and superconductivity [2] emerge for small carrier densities around charge neutrality. Other interesting phases such as anomalous Hall ferromagnetism [3,4] or fractional Chern numbers have also been observed [5–7]. These phenomena are related to the flat bands around charge neutrality that have been predicted theoretically [8,9].

Since then, the study of twisted geometries of van der Waals heterostructures, often referred to as moiré materials [10], has become an active area of research. The subjects of these investigations include twisted bilayers composed of various transition metal dichalcogenides [11–18], aside from the twisted bilayer graphene. Moreover, the number of sheets in moiré graphene systems has been increased to up to five alternately twisted layers [19,20]. Recently, also quasi-three-dimensional twisted structures were fabricated, which exhibit an intrinsic enhanced chirality [21,22].

Lately, special emphasis has been placed on the study of the twisted trilayer graphene [23–41]. This is the minimal system that can form not only quasicommensurate but also incommensurate structures. Quasicommensurate structures can be described by two moiré vectors, whereas incommensurate structures are usually described by four moiré vectors: two for each of the moiré lattices that are formed by the two pairs of consecutive layers (say, layers 1 and 2, and layers 2 and 3, respectively) [27,42–45]. Interestingly, superconductivity has been found in both types of structures, that is, commensurate [23–25,40] and incommensurate trilayer structures [46,47].

Notably, optical experiments on moiré systems have also attracted considerable attention [48–51]. A goal is to control the phase, amplitude, or polarization state of light from the response of multilayered structures.

In this paper, we analytically study the electromagnetic response of the twisted trilayer graphene. Our approach is based on symmetry considerations and microscopic principles of linear response theory. We focus on the alternating-twist configuration, in which $\theta_{12} = -\theta_{23}$ where θ_{ij} denotes the angle between layers i and j. In this case, in the presence of mirror symmetry with respect to the central layer, also preserved after including in-plane and out-of-plane relaxation [52], we show that the in-plane magnetic response is negligibly small. By mirror symmetry, there is no optical activity; however, we formulate a local magnetoelectric (chiral) coupling that involves vertical gradients of the magnetic field and moment.

In our analysis, we make use of a unitary transformation, introduced in Ref. [53], that converts the trilayer system into a combination of effective twisted bilayer and single-layer systems. Linear response theory for the trilayer eventually couples these two systems. We derive a formula for this coupling, and estimate its magnitude. We also describe, in terms of contributions from these two systems, the layer-resolved conductivities that enter the optical response. In particular, we analytically show how the in-plane magnetic response arises from the coupling of the two effective systems.

The alternating-twist trilayer system under mirror symmetry investigated here is one of the most stable layered structures, minimizing the configuration stacking fault energy. This remarkable mechanical stability renders this system prototypical, and is another motivation for our work. Furthermore, in the Appendices we extend the analysis for the optical conductivity to alternating-twist trilayers in which the mirror symmetry with respect to the middle layer is broken because of the different interlayer tunneling.

A highlight of our results is the connection of the optical response of the trilayer system to microscopic parameters of

---

*Contact author: diom@umd.edu
†Contact author: guillermo.gomez@uam.es
‡Contact author: tobias.stauber@csic.es

effective Hamiltonians for simpler systems. Thus, we are able to illustrate the important role of the large moiré length. For example, the effect of this scale renders negligible the relative contribution of the in-plane magnetic response. In this paper, we focus on analytical predictions that explicitly reveal the interplay of two scales in the optical response. Hence, we choose not to use or rely on numerical simulations in this work.

The remainder of the paper is organized as follows. Section II focuses on the conductivity tensor via the Kubo formulation. In particular, we discuss the roles of the effective twisted bilayer and single-layer systems and the coupling term between them. In Sec. III, we formulate the optical response in terms of an in-plane electric moment and the vertical gradient of the in-plane magnetic moment, which are coupled. In Sec. IV, we discuss the in-plane magnetic response by giving an analytical expression and estimates. In Sec. V, we conclude the paper with a summary of our main results. The Appendices mainly provide technical derivations relevant to the main text.

Throughout the paper, boldface symbols denote vectors or matrices that pertain to the (x and y) directions of the reference plane. The $e^{-i\omega t}$ time dependence is assumed (ω is the frequency).

II. MICROSCOPIC THEORY FOR LAYER-RESOLVED CONDUCTIVITIES

In this section, we provide key ingredients and results of the Kubo formulation for the trilayer system. The general layer-resolved response theory in the frequency domain for a system with n layers is given by [54,55]

$$\mathbf{J}_\ell = \sum_{\ell'=1}^{n} \boldsymbol{\sigma}^{\ell\ell'} \mathbf{E}_{\ell'} \quad (\ell = 1, \ldots, n), \tag{1}$$

where $\mathbf{J}_\ell$ and $\mathbf{E}_\ell$ denote the macroscopic surface current density and electric field in layer ℓ, respectively. The 2×2 matrices $\boldsymbol{\sigma}^{\ell\ell'}(\omega)$ have elements defined by $\sigma_{\nu\nu'}^{\ell\ell'}(\omega) = i\frac{e^2}{\omega+i\delta}\chi_{\nu\nu'}^{\ell\ell'}(\omega + i\delta)$, as $\delta \downarrow 0$, with the current-current response function

$$\chi_{\nu\nu'}^{\ell\ell'}(\omega) = -\frac{i}{\hbar}\int_0^\infty dt\, e^{i\omega t}\langle[j_\nu^\ell(t), j_{\nu'}^{\ell'}(0)]\rangle, \tag{2}$$

where $j_\nu^\ell(t)$ is the ν-directed current operator ($\nu = x, y$) in layer ℓ in the interaction picture, and $\langle\cdot\rangle$ is the equilibrium average.

Here, we consider a moiré multilayer with $n = 3$. The geometry of the alternating-twist trilayer system is shown in Fig. 1. The twist angle of layer ℓ is $\theta_\ell = (-1)^\ell\theta/2$ where $0 < \theta < \pi/2$ and $\ell = 1, 2, 3$; the interlayer distance is $a/2$. Furthermore, we mainly consider a mirror-symmetric configuration. Hence, the matrices $\boldsymbol{\sigma}^{\ell\ell'}$ satisfy $\boldsymbol{\sigma}^{11} = \boldsymbol{\sigma}^{33}$, $\boldsymbol{\sigma}^{12} = \boldsymbol{\sigma}^{32}$, and $\boldsymbol{\sigma}^{21} = \boldsymbol{\sigma}^{23}$.

Let us recall that the symmetry group of the twisted bilayer system is D_3 [56]. However, by the mirror symmetry of the alternating-twist trilayer, the symmetry group now is D_{3h}. This additional symmetry doubles the number of representations, i.e., we have four one-dimensional and two two-dimensional representations in total.
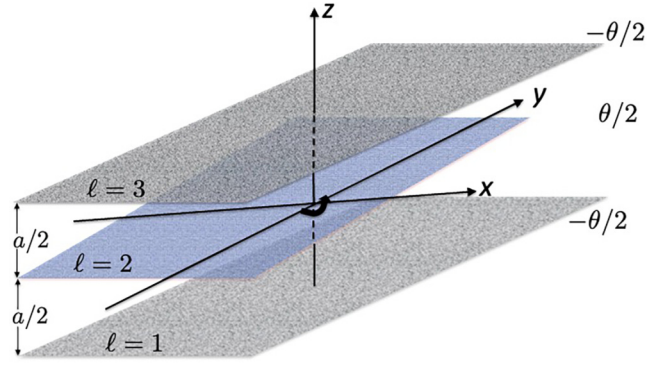

FIG. 1. Schematic of the alternating-twist trilayer configuration. Three infinite flat graphene sheets labeled by $\ell = 1, 2, 3$ are parallel to the xy plane, and have twist angles $(-1)^\ell\theta/2$ and interlayer distance equal to $a/2$ ($0 < \theta < \pi/2$). The layers are immersed in a homogeneous medium.

Due to the rotational (threefold) symmetry of the system, we can write each 2×2 conductivity matrix as follows [54]:

$$\boldsymbol{\sigma}^{\ell\ell'} = \sigma_0^{\ell\ell'}\mathbf{1} + i\sigma_{xy}^{\ell\ell'}\boldsymbol{\tau}_y, \tag{3}$$

where $\boldsymbol{\tau}_y$ denotes the y-Pauli matrix. Because of the mirror symmetry of the trilayer configuration, we only have four independent response functions, namely, σ_0^{11}, σ_0^{12}, σ_0^{13}, and σ_0^{22}. These are related to the four one-dimensional representations of the group D_{3h}.

Moreover, time-reversal symmetry implies $\sigma_{\nu\nu'}^{\ell\ell'} = \sigma_{\nu'\nu}^{\ell'\ell}$ (see Appendix A). Because of time-reversal and mirror symmetries, we may further include the parameters σ_{xy}^{12} and σ_{xy}^{13}, which are related to the two two-dimensional representations of D_{3h}. These parameters can give rise to chiral phenomena such as circular dichroism [48,51,57,58] and layer-resolved Hall physics in the dc limit [59,60]. Here, $\sigma_{xy}^{13} = 0$ since we consider the $\mathbf{q} = 0$ response and the first and third layers have the same orientation (see Fig. 1). The parameter σ_{xy}^{12} will be kept finite; however, no chiral response can emerge due to the inherent mirror symmetry. Still, we can formulate constitutive equations that involve σ_{xy}^{12} and lead to *local* chirality (see Sec. III).

A. Kubo formalism

By Eq. (2), the surface conductivity matrix elements in the frequency domain are given by

$$\sigma_{\nu\nu'}^{\ell\ell'}(\omega) = \frac{e^2}{\hbar(\omega + i\delta)}\sum_{\{|\psi\rangle\}} f(E_\psi)$$
$$\times \int_0^\infty dt\, e^{i(\omega+i\delta)t}\langle\psi|[j_\nu^\ell(t), j_{\nu'}^{\ell'}(0)]|\psi\rangle, \tag{4}$$

as $\delta \downarrow 0$, for real frequencies ω ($\ell, \ell' = 1, 2, 3$ and $\nu, \nu' = x, y$). Here, $|\psi\rangle$ is any normalized eigenvector of the trilayer Hamiltonian with eigenvalue E_ψ and $f(E)$ is the Fermi-Dirac distribution. Regarding the K valley, we use the Hamiltonian $\mathcal{H}_K^{\text{tri}}$ of Appendix B; and symmetrize the ensuing conductivity because of time-reversal symmetry (Appendix A). In Eq. (4), $j_\nu^\ell(t)$ has dimensions of inverse time, or frequency.

To describe the K-valley term $\sigma_{\nu\nu',K}^{\ell\ell'}$, we rewrite Eq. (4) by unitarily transforming each eigenvector $|\psi\rangle$, while $\mathcal{H}_K^{\text{tri}}$ is transformed into the direct sum of the single-layer and effective twisted bilayer Hamiltonians $\mathcal{H}_1$ and $\mathcal{H}_2$, respectively; see Eqs. (B14) and (B15) in Appendix B. The transformed eigenvectors of $\mathcal{H}_K^{\text{tri}}$ are $|\underline{\psi}\rangle = \mathfrak{S}^\dagger|\psi\rangle$, where $\mathfrak{S}$ is defined in Eq. (B12) or (B13) (Appendix B); and are related to either the effective twisted bilayer or single-layer Hamiltonian

$$|\underline{\psi}\rangle_b = \begin{pmatrix} |b\rangle_1 \\ |b\rangle_2 \\ 0 \end{pmatrix}, \quad |\underline{\psi}\rangle_s = \begin{pmatrix} 0 \\ 0 \\ |s\rangle \end{pmatrix}, \quad (5)$$

where $(|b\rangle_1, |b\rangle_2)^T$ and $|s\rangle$ denote any normalized-to-unity eigenvector of the effective bilayer Hamiltonian $\mathcal{H}_2$ and monolayer Hamiltonian $\mathcal{H}_1$, respectively. Each of the indices b and s amounts to the combined band index and quasimomentum of the moiré Brillouin zone, and $\langle \boldsymbol{x}|\underline{\psi}\rangle$ consists of Bloch functions. We thus have

$$\mathcal{H}_2 \begin{pmatrix} |b\rangle_1 \\ |b\rangle_2 \end{pmatrix} = E_b \begin{pmatrix} |b\rangle_1 \\ |b\rangle_2 \end{pmatrix}, \quad \mathcal{H}_1|s\rangle = E_s|s\rangle.$$

By this notation, Eq. (4) becomes

$$\sigma_{\nu\nu',K}^{\ell\ell'}(\omega) = \frac{e^2}{\hbar(\omega+i\delta)} \int_0^\infty dt\, e^{i(\omega+i\delta)t}$$

$$\times \left\{ \sum_b f(E_b)_b\langle\underline{\psi}|\big[\underline{j}_{\nu,K}^\ell(t), \underline{j}_{\nu',K}^{\ell'}(0)\big]|\underline{\psi}\rangle_b \right.$$

$$\left. + \sum_s f(E_s)_s\langle\underline{\psi}|\big[\underline{j}_{\nu,K}^\ell(t), \underline{j}_{\nu',K}^{\ell'}(0)\big]|\underline{\psi}\rangle_s \right\}, \quad (6)$$

where $\underline{j}_{\nu,K}^\ell = \mathfrak{S}^\dagger j_{\nu,K}^\ell \mathfrak{S}$. For details, see Appendix C.

B. Transforming conductivity tensor via mirror symmetry

Next, we focus on the mirror-symmetric setting, where the electron tunneling for layers 1, 2 is the same as that for layers 2, 3. In Appendix C, we discuss the more general setting without mirror symmetry by keeping the alternating twists, using $\theta_{12} = -\theta_{23}$.

Let $\boldsymbol{\sigma}_{\text{BL}}^{\varsigma\varsigma'}$ ($\varsigma, \varsigma' = 1, 2$) and $\boldsymbol{\sigma}_{\text{SL}}$ denote the 2×2 conductivity block matrices of the effective twisted bilayer and single-layer systems. These quantities have been discussed in previous work [54], and can be considered as known. In Appendix C, they are expressed in terms of matrix elements of pseudo-spin-wave functions.

The connection between the trilayer response and $\boldsymbol{\sigma}_{\text{BL}}^{\varsigma\varsigma'}$ and $\boldsymbol{\sigma}_{\text{SL}}$ can be obtained by applying to the currents the following transformation:

$$\begin{pmatrix} \tilde{\mathbf{J}}_1 \\ \tilde{\mathbf{J}}_2 \\ \tilde{\mathbf{J}}_3 \end{pmatrix} = \begin{pmatrix} \frac{1}{\sqrt{2}} & 0 & \frac{1}{\sqrt{2}} \\ 0 & 1 & 0 \\ \frac{1}{\sqrt{2}} & 0 & -\frac{1}{\sqrt{2}} \end{pmatrix} \begin{pmatrix} \mathbf{J}_1 \\ \mathbf{J}_2 \\ \mathbf{J}_3 \end{pmatrix}. \quad (7)$$

The electric fields are transformed by the same matrix into $(\tilde{\mathbf{E}}_1, \tilde{\mathbf{E}}_2, \tilde{\mathbf{E}}_3)$. The transformation for the current densities here follows directly from the conversion of the trilayer Hamiltonian into a direct sum of effective Hamiltonians (Appendix B). By the microscopic analysis of Appendix C, results of which

we show below, the layer-resolved response implies a relation of the form

$$\begin{pmatrix} \tilde{\mathbf{J}}_1 \\ \tilde{\mathbf{J}}_2 \\ \tilde{\mathbf{J}}_3 \end{pmatrix} = \frac{1}{2} \begin{pmatrix} (\boldsymbol{\sigma}_{\text{BL}}^{11} + \boldsymbol{\sigma}_{SL}) & \sqrt{2}\boldsymbol{\sigma}_{\text{BL}}^{12} & 0 \\ \sqrt{2}\boldsymbol{\sigma}_{\text{BL}}^{21} & 2\boldsymbol{\sigma}_{\text{BL}}^{22} & 0 \\ 0 & 0 & \boldsymbol{\sigma}_c \end{pmatrix} \begin{pmatrix} \tilde{\mathbf{E}}_1 \\ \tilde{\mathbf{E}}_2 \\ \tilde{\mathbf{E}}_3 \end{pmatrix}, \quad (8)$$

where

$$\boldsymbol{\sigma}_{\text{SL}} = \sigma_e^{(1)}\mathbf{1}, \quad \boldsymbol{\sigma}_{\text{BL}}^{11} = \boldsymbol{\sigma}_{\text{BL}}^{22} = \sigma_e^{(2)}\mathbf{1}, \quad \boldsymbol{\sigma}_c = \sigma_c\mathbf{1},$$

$$\boldsymbol{\sigma}_{\text{BL}}^{12} = \big(\boldsymbol{\sigma}_{\text{BL}}^{21}\big)^T = \sigma_e^{12}\mathbf{1} + i\sigma_{e,xy}^{12}\boldsymbol{\tau}_y.$$

Here, we introduced the scalar functions $\sigma_e^{(\varsigma)}(\omega)$, $\sigma_e^{12}(\omega)$, $\sigma_{e,xy}^{12}(\omega)$, and $\sigma_c(\omega)$, to be described in Sec. II C. The above matrix forms account for time-reversal symmetry and isotropy (see Appendix C).

By transforming Eq. (8) back to the layer-resolved response of Eq. (1), we identify the $\boldsymbol{\sigma}^{\ell\ell'}$ matrices as follows ($\ell, \ell' = 1, 2, 3$):

$$\boldsymbol{\sigma}^{11} = \tfrac{1}{4}\big(\boldsymbol{\sigma}_{\text{BL}}^{11} + \boldsymbol{\sigma}_{\text{SL}} + \boldsymbol{\sigma}_c\big), \quad (9)$$

$$\boldsymbol{\sigma}^{13} = \tfrac{1}{4}\big(\boldsymbol{\sigma}_{\text{BL}}^{11} + \boldsymbol{\sigma}_{\text{SL}} - \boldsymbol{\sigma}_c\big), \quad (10)$$

$$\boldsymbol{\sigma}^{12} = \tfrac{1}{2}\boldsymbol{\sigma}_{\text{BL}}^{12}, \quad \boldsymbol{\sigma}^{22} = \boldsymbol{\sigma}_{\text{BL}}^{22}. \quad (11)$$

The other components are obtained by mirror and time-reversal symmetries [cf. Eq. (3)].

From the above equations, the optical responses of Eq. (1) can thus be expressed in terms of $\sigma_e^{(1,2)}$, $\sigma_{e(,xy)}^{12}$, and σ_c. Except for σ_c, these conductivities are known, in principle, from the electromagnetic responses of the isolated single-layer and twisted bilayer graphene [54]. In contrast, σ_c stands out because, even though the trilayer Hamiltonian decouples into effective single-layer and bilayer systems, the currents involved in σ_c mix both of these subsystems.

C. Explicit expressions for conductivities

We now describe the parameters of $\boldsymbol{\sigma}_{\text{BL}}^{\varsigma\varsigma'}$, $\boldsymbol{\sigma}_{\text{SL}}$, and $\boldsymbol{\sigma}_c$ via inner products of pseudo-spin-wave functions. For notational convenience, let $\boldsymbol{\tau}_\pm = \frac{1}{2}(\boldsymbol{\tau}_x \pm i\boldsymbol{\tau}_y)$ where $\tau_{x,y}$ are the x, y components of the Pauli matrices.

First, the matrix $\boldsymbol{\sigma}_c(\omega)$ emerges from the overlap of Bloch eigenvectors of the two effective systems in the Kubo trace formula. By $\boldsymbol{\sigma}_c = \text{diag}(\sigma_c, \sigma_c)$, we derive

$$\sigma_c = -i2g_v g_s \frac{v_F^2}{A_m} \frac{e^2}{\hbar(\omega+i\delta)} \sum_{bs} \frac{(f_b - f_s)\omega_{bs}}{(\omega+i\delta)^2 - \omega_{bs}^2}$$

$$\times (|_1\langle b|\tau_+|s\rangle|^2 + |_1\langle b|\tau_-|s\rangle|^2), \quad (12)$$

where $\omega_{bs} = (E_b - E_s)/\hbar$, $f_{b(s)} = f(E_{b(s)})$, g_v (g_s) is the valley (spin) degeneracy factor, v_F is the Fermi velocity of monolayer graphene, and A_m is the area of the reference moiré cell (see Appendix C). This expression is simplified in view of $|_1\langle b|\tau_+|s\rangle|^2 = |_1\langle b|\tau_-|s\rangle|^2$ because of a symmetry of the effective Hamiltonians $\mathcal{H}_{1,2}$ under the interchange of the sublattice indices. The relative magnitude of σ_c is estimated in Sec. IV.

We will now discuss the response functions, also present in the bilayer system [54]. The first element is the chirality

parameter σ_{xy}^{12} from the effective bilayer system. This equals

$$\sigma_{xy}^{12}(\omega) = \frac{1}{2}\sigma_{e,xy}^{12} = i g_v g_s \frac{v_F^2}{A_m} \frac{e^2}{\hbar(\omega + i\delta)} \sum_{bb'} (f_b - f_{b'})$$

$$\times \frac{\omega_{bb'} \operatorname{Im}\{e^{-i\theta}(_2\langle b'|\tau_-|b\rangle_2)(_1\langle b|\tau_+|b'\rangle_1)\}}{(\omega + i\delta)^2 - \omega_{bb'}^2}, \quad (13)$$

where $\omega_{bb'} = (E_b - E_{b'})/\hbar$. For $\theta = 0$, σ_{xy}^{12} must vanish. This property is derived by noting that for $\theta = 0$ we have $_1\langle b|\tau_\pm|b'\rangle_1 = {}_2\langle b|\tau_\pm|b'\rangle_2$, switching layers in $\mathcal{H}_2$, where $_{1(2)}\langle b|\tau_\pm|b'\rangle_{1(2)} = (_{1(2)}\langle b'|\tau_\mp|b\rangle_{1(2)})^*$. More generally, we have $\sigma_{xy}^{12}(\omega; \theta) = -\sigma_{xy}^{12}(\omega; -\theta)$ (see also Ref. [54]).

The remaining response parameters are given by

$$\sigma_e^{(1)} = -i2g_v g_s \frac{v_F^2}{A_m} \frac{e^2}{\hbar(\omega + i\delta)} \sum_{ss'} \frac{(f_s - f_{s'})\omega_{ss'}}{(\omega + i\delta)^2 - \omega_{ss'}^2}$$

$$\times |\langle s|\tau_+|s'\rangle|^2, \quad (14)$$

$$\sigma_e^{(2)} = -i g_v g_s \frac{v_F^2}{A_m} \frac{e^2}{\hbar(\omega + i\delta)} \sum_{bb'} \frac{(f_b - f_{b'})\omega_{bb'}}{(\omega + i\delta)^2 - \omega_{bb'}^2}$$

$$\times (|_1\langle b|\tau_+|b'\rangle_1|^2 + |_2\langle b'|\tau_-|b\rangle_2|^2), \quad (15)$$

$$\sigma_e^{12} = -i2g_v g_s \frac{v_F^2}{A_m} \frac{e^2}{\hbar(\omega + i\delta)} \sum_{bb'} \frac{(f_b - f_{b'})\omega_{bb'}}{(\omega + i\delta)^2 - \omega_{bb'}^2}$$

$$\times \operatorname{Re}\{e^{-i\theta}(_1\langle b|\tau_+|b'\rangle_1)(_2\langle b'|\tau_-|b\rangle_2)\}. \quad (16)$$

By Eqs. (15) and (16), regarding the effective bilayer system, we can show that $\sigma_e^\eta(\omega; \theta) = \sigma_e^\eta(\omega; -\theta)$ (see also Ref. [54]).

III. COUPLING BETWEEN ELECTRIC AND LOCAL MAGNETIC FIELDS

In the preceding analysis, we have formulated the linear response in terms of conductivities. However, the emergence of chiral effects is often described in terms of a coupled response to electric and magnetic fields.

For even modes, the trilayer responses can be read off from the responses of the single-layer graphene and twisted bilayer graphene, which are already known [see Eq. (8)]. Given the chiral nature of twisted bilayer graphene, and to make contact with Ref. [54], we will also employ a magnetic language. Notice, though, that the mirror-symmetric trilayer does not exhibit optical activity. Therefore, even though some equations for the trilayer will look formally very similar to those of the twisted bilayer graphene [54], magnetic moments and magnetic fields will enter through layer differences, considered as "gradients" in the z direction, to comply with space-inversion symmetry [58].

A. Modes under mirror symmetry

We define the following transformation of the original electric fields that will relate the current response to effective electric and magnetic dipoles:

$$\begin{pmatrix} \mathcal{E}_+^+ \\ \mathcal{E}_+^- \\ \mathcal{E}_- \end{pmatrix} = M \begin{pmatrix} \mathbf{E}_1 \\ \mathbf{E}_2 \\ \mathbf{E}_3 \end{pmatrix}, \quad (17)$$

with

$$M = \begin{pmatrix} \sqrt{1/3} & \sqrt{1/3} & \sqrt{1/3} \\ \sqrt{1/6} & -\sqrt{2/3} & \sqrt{1/6} \\ \sqrt{1/2} & 0 & -\sqrt{1/2} \end{pmatrix}. \quad (18)$$

In the above matrix, each entry expresses a 2×2 block matrix. Up to normalizing constants, this matrix can be understood as follows: The first row is the layer-averaged field, the second row is the (layer-discrete) second derivative of the field, and the third row is the (layer-discrete) first derivative of the field.

The original current densities are transformed in the same fashion as the original electric fields [Eq. (17)], according to the equation

$$\begin{pmatrix} \mathcal{J}_+^+ \\ \mathcal{J}_+^- \\ \mathcal{J}_- \end{pmatrix} = M \begin{pmatrix} \mathbf{J}_1 \\ \mathbf{J}_2 \\ \mathbf{J}_3 \end{pmatrix}. \quad (19)$$

Since the total system is mirror symmetric, the odd mode $\mathcal{J}_-$ is again decoupled from the two even modes. Thus, we obtain the following relations:

$$\left.\begin{aligned} \mathcal{J}_+^+ &= \sigma_+^+ \mathcal{E}_+^+ + \sqrt{2}\sigma_+^{+-}\mathcal{E}_+^- + \sqrt{2}\sigma_{xy}^{12}(\mathbf{e}_z \times \mathcal{E}_+^-), \\ \mathcal{J}_+^- &= \sigma_+^- \mathcal{E}_+^- + \sqrt{2}\sigma_+^{+-}\mathcal{E}_+^+ - \sqrt{2}\sigma_{xy}^{12}(\mathbf{e}_z \times \mathcal{E}_+^+), \\ \mathcal{J}_- &= (\sigma_{11}^0 - \sigma_{13}^0)\mathcal{E}_-. \end{aligned}\right\} \quad (20)$$

Here, $\mathbf{e}_z$ is the z-directed Cartesian unit vector, and

$$\left.\begin{aligned} 3\sigma_+^+ &= 2(\sigma_0^{11} + \sigma_0^{13}) + \sigma_0^{22} + 4\sigma_0^{12}, \\ 3\sigma_+^- &= (\sigma_0^{11} + \sigma_0^{13}) + 2\sigma_0^{22} - 4\sigma_0^{12}, \\ 3\sigma_+^{+-} &= (\sigma_0^{11} + \sigma_0^{13}) - \sigma_0^{22} - \sigma_0^{12}. \end{aligned}\right\} \quad (21)$$

Recall that by Eqs. (9)–(11) the conductivities $\sigma_0^{\ell\ell'}$ are expressed in terms of the effective single-layer and twisted bilayer responses. Furthermore, we have $\sigma_c = 2(\sigma_{11}^0 - \sigma_{13}^0)$ from Eqs. (9) and (10).

B. Effective local description for modes

Let us now focus on the modes that define the response of the trilayer. We can formulate the constitutive equations with respect to electric and local magnetic fields [54]. From the discrete (layer-resolved) version of Maxwell's equations, we write

$$\mathbf{E}_\parallel = (\mathbf{E}_1 + \mathbf{E}_2 + \mathbf{E}_3)/3, \quad (22)$$

$$i\omega(a/2)\mathbf{B}_\parallel^{12} = \mathbf{e}_z \times (\mathbf{E}_2 - \mathbf{E}_1), \quad (23)$$

$$i\omega(a/2)\mathbf{B}_\parallel^{23} = \mathbf{e}_z \times (\mathbf{E}_3 - \mathbf{E}_2). \quad (24)$$

Equation (22) is the average electric field. Equations (23) and (24) are discrete versions of the Maxwell-Faraday law (or, the third Maxwell equation). Therefore, $\mathbf{B}_\parallel^{\ell\ell'}$ is the (average) magnetic field between layers ℓ and ℓ'. For mirror-symmetric modes, when $\mathbf{E}_1 = \mathbf{E}_3$, there is no net magnetic field, i.e., $\mathbf{B}_\parallel^{12} + \mathbf{B}_\parallel^{23} = 0$. Nevertheless, a finite value of $\mathbf{B}_\parallel^{12}$ ($\mathbf{B}_\parallel^{23}$) can be viewed as a vertical gradient of the magnetic field, as previously noted.
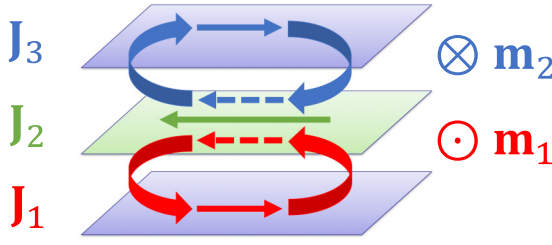
FIG. 2. Schematic view of the currents when only the even mode $\mathcal{J}_+^-$ is present; see Eqs. (18) and (19). The solid arrows define the in-plane current densities $\mathbf{J}_1$, $\mathbf{J}_2$, and $\mathbf{J}_3$ with $\mathbf{J}_1 = \mathbf{J}_3 = -\mathbf{J}_2/2$. These currents give rise to the magnetic moments $\mathbf{m}_1$ and $\mathbf{m}_2$ with $\mathbf{m}_1 = -\mathbf{m}_2$.

The in-plane original current densities can always be described in terms of electric and magnetic moments, as explained in Appendix D. For the trilayer, the relations are

$$-i\omega\mathbf{p} = \mathbf{J}_1 + \mathbf{J}_2 + \mathbf{J}_3, \tag{25}$$

$$\frac{\mathbf{m}_2 - \mathbf{m}_1}{a/6} = \mathbf{e}_z \times (\mathbf{J}_3 + \mathbf{J}_1 - 2\mathbf{J}_2), \tag{26}$$

$$\frac{\mathbf{m}_1 + \mathbf{m}_2}{a/2} = \mathbf{e}_z \times (\mathbf{J}_3 - \mathbf{J}_1). \tag{27}$$

The linear combinations of currents in Eqs. (25)–(27) correspond to the modes $\mathcal{J}_+^+$, $\mathcal{J}_+^-$, and $\mathcal{J}_-$, respectively. In

the absence of a net current, if $\mathbf{p} = 0$, the in-plane current densities of modes $\{\mathcal{J}_+^-, \mathcal{J}_-\}$ can thus be thought of as magnetization currents associated with a uniform magnetization $\mathbf{m}_1$, filling the space between layers 1 and 2, and magnetization $\mathbf{m}_2$, filling the space between layers 2 and 3. Equations (26) and (27) then follow, as shown in Appendix D.

For mirror-symmetric modes, when $\mathbf{J}_1 = \mathbf{J}_3$, no net magnetic moment exists, i.e., $\mathbf{m}_1 + \mathbf{m}_2 = 0$. Nevertheless, the finite value of $\mathbf{m}_1$ ($\mathbf{m}_2$) can be viewed as a gradient of the magnetic moment, as previously mentioned. The local magnetic moments of the mode $\mathcal{J}_+^-$ are shown in Fig. 2. This mode is even in the current density, but odd in the magnetic moment.

Therefore, by introducing the vertical gradients of the magnetic field and moment as

$$\Delta\mathbf{B}_\parallel = (\mathbf{B}_\parallel^{23} - \mathbf{B}_\parallel^{12})/2, \tag{28}$$

$$\Delta\mathbf{m} = \mathbf{m}_2 - \mathbf{m}_1, \tag{29}$$

and noticing that

$$\mathbf{B}_\parallel = (\mathbf{B}_\parallel^{23} + \mathbf{B}_\parallel^{12})/2, \tag{30}$$

$$\mathbf{m}_\parallel = \mathbf{m}_1 + \mathbf{m}_2, \tag{31}$$

we can formulate the following constitutive law:

$$\begin{pmatrix} \mathbf{p} \\ \Delta\mathbf{m} \\ \mathbf{m}_\parallel \end{pmatrix} = \begin{pmatrix} -3\sigma_+^+/(i\omega) & a\{\sigma_+^{+-}(\mathbf{e}_z \times \cdot) - \sigma_{xy}^{12}\} & 0 \\ a\{\sigma_+^{+-}(\mathbf{e}_z \times \cdot) + \sigma_{xy}^{12}\} & i\omega(a^2/6)\sigma_+^- & 0 \\ 0 & 0 & i\omega(a^2/4)\sigma_c \end{pmatrix} \begin{pmatrix} \mathbf{E}_\parallel \\ \Delta\mathbf{B} \\ \mathbf{B}_\parallel \end{pmatrix}. \tag{32}$$

Finally, we should point out that although the system is mirror symmetric and does not exhibit optical activity, the xy component σ_{xy}^{12} of the response introduces a local "chiral coupling" between the electric field and the gradient of the magnetic field.

IV. IN-PLANE MAGNETIC RESPONSE

In this section, we derive a simplified formula for the in-plane magnetic response, and estimate it as negligibly small. As shown in Sec. III B, the in-plane magnetic response is given by

$$\mathbf{m}_\parallel = i\omega\frac{a^2}{4}\sigma_c\mathbf{B}_\parallel. \tag{33}$$

We repeat that the magnetic-response parameter σ_c cannot be read from the responses of the isolated single-layer and twisted bilayer systems. However, mainly because of the kinematic constraints arising from the largely different Fermi velocities in these two systems, we expect σ_c to be practically zero. In this section, we verify this property analytically.

The small, almost vanishing in-plane magnetic response of twisted trilayer graphene is in stark contrast to the large in-plane magnetic response of the twisted bilayer graphene [54]. The latter can even diverge and give rise to a Condon instability [56,61].

A. Microscopic derivation and localization ansatz

We will derive an explicit, simplified formula for the in-plane magnetic response, Eq. (33), near charge neutrality for alternating twists close to the magic angle. For this purpose, we introduce the following parameter of the in-plane magnetic response:

$$\chi_m^c(\omega) = i\omega\frac{a^2}{4}\sigma_c(\omega). \tag{34}$$

We need to estimate the coupling term σ_c, or response χ_m^c. For this task, we employ a localization ansatz for the electronic Bloch wave functions of the effective twisted bilayer system at nearly flat bands, in the spirit of Ref. [62].

Consider the eigenstates of Eq. (5). For the effective bilayer system, our localization hypothesis reads as [62]

$$\begin{pmatrix} \langle \mathbf{x}|b\rangle_1 \\ \langle \mathbf{x}|b\rangle_2 \end{pmatrix} \simeq e^{i(\mathbf{K}+\mathbf{q})\cdot\mathbf{x}}\Phi_n(\sqrt{\xi}\mathbf{x}/L_m)\begin{pmatrix} P_{1,n} \\ P_{2,n} \end{pmatrix} \tag{35}$$

near the K point. Here, $P_{\ell,n}$ is a 2×1 vector for the sublattice polarization in each layer ($\ell = 1, 2$), n is the band index (e.g., $n = \pm1$ for flat bands), L_m is the moiré length ($|\mathbf{K}|L_m \gg 1$), $\mathbf{q}$ is the quasimomentum vector ($q \ll |\mathbf{K}|$), and $\xi \simeq 3$ [62]. The function Φ_n is localized in the moiré cell. By normalizing

formula (35) with $|P_{1,n}| \sim |P_{2,n}|$ we obtain

$$P_{\ell,n} \sim e^{i\vartheta_{\ell,n}} \sqrt{\frac{\xi}{4L_m^2}} \begin{pmatrix} 1 \\ 1 \end{pmatrix}, \qquad (36)$$

where $\vartheta_{\ell,n}$ is a phase that does not affect our results, and Φ_n is normalized to unity. The symbol $\sim$ means that numerical factors roughly equal to unity or smaller are ignored for the sake of order-of-magnitude estimates. The eigenvectors of the single-layer system are

$$\langle x|s \rangle = \frac{1}{\sqrt{2A_m}} e^{i(\mathbf{K}+q)\cdot x} \begin{pmatrix} 1 \\ \pm e^{i\theta/2} \frac{q_x + iq_y}{q} \end{pmatrix} \qquad (37)$$

for its two bands, where $A_m \sim L_m^2$.

Let us invoke Eqs. (35) and (37) in Eq. (12). We assume that $\omega < v_F q_m$ with $q_m = \frac{2\pi}{L_m}$. By only considering the nearly flat bands for the effective bilayer system, and relatively large energies of the effective monolayer system so that $\omega_b - \omega_s \simeq -\omega_s$, we have

$$\chi_m^c \sim \frac{g_v g_s}{2(4\pi)^2} v_F^2 a^2 \frac{e^2}{\hbar} \sum_{n,n_s = \pm 1} |\bar{C}_n(\xi)|^2 \int_{\text{mBZ}} dq$$
$$\times [f(E_n^b) - f(E_{n_s})] \frac{n_s v_F q}{(v_F q)^2 - (\omega + i\delta)^2}. \qquad (38)$$

In the above, the integration region mBZ is the moiré Brillouin zone, $E_n^b(q)$ [$E_{n_s}(q)$] is the energy of the effective bilayer (single-layer) system at band n (n_s), and

$$\bar{C}_n(\xi) = \frac{1}{\sqrt{\xi}} \int dx' \, \Phi_n(x') \quad (n = \pm 1)$$

over the transformed moiré cell by $x \mapsto x' = \frac{\sqrt{\xi}}{L_m} x$. The scaling of this integral with $\sqrt{\xi}$ ensures that $|\bar{C}_n| \lesssim 1$ regardless of the value of $\xi > 0$.

B. Estimate for the magnetic response

We will now evaluate the integral for the parameter χ_m^c by neglecting terms proportional to or smaller than $\frac{\omega}{v_F q_m} \ln(\frac{v_F q_m}{\omega})$; thus, $\hbar\omega$ may not exceed a few hundred meV which poses no practical restriction.

To demonstrate that χ_m^c is negligibly small, we compare it to $\chi_0 = \hbar^{-2} e^2 t_G a_C^2$, which is used in discussions about lattice effects on the out-of-plane magnetic susceptibility in the single-layer graphene [63]. Here, a_C is the carbon-carbon distance and t_G is the hopping energy for monolayer graphene. Hence, we compute

$$\frac{\chi_m^c}{\chi_0} \sim \frac{3}{8} g_v g_s \langle f \rangle_m^c \frac{a^2/a_C}{L_m} \simeq 1.2 \langle f \rangle_m^c \qquad (39)$$

with $a = 1$ nm $\simeq 7a_C$, $L_m = a_C \sqrt{3} \sqrt{3i^2 + 3i + 1} \simeq 61.43 a_C$ for $i = 20$, regarding the trilayer configuration (Fig. 1). Here, we assume that the alternating-twist trilayer is in the magic-angle regime.

Notice the linear scaling of $\frac{\chi_m^c}{\chi_0}$ with the inverse moiré length. The positive factor $\langle f \rangle_m^c$ depends on the $|\bar{C}_n|$'s of nearly flat bands and the Fermi-Dirac distribution f, and expresses a weighted radial-momentum average of $f(E_-(q)) -$

$f(E_+(q))$ for the single-layer graphene energies $E_\pm(q) = \pm \hbar v_F q$. This average is defined by

$$\langle f \rangle_m^c = \frac{1}{2} (|\bar{C}_1|^2 + |\bar{C}_{-1}|^2)$$
$$\times \left\{ \frac{1}{q_m} \int_0^{q_m} dq \, [f(E_-(q)) - f(E_+(q))] \right\}.$$

Note that $\langle f \rangle_m^c < 1$.

Equation (39) suggests that the in-plane magnetic response of the alternating twisted trilayer is very weak since it is comparable to or smaller than the corresponding atomistic (lattice) effect in monolayer graphene. Evidently, the response function $\chi_m^c(\omega)$ has a plateau in frequency for $\omega \lesssim v_F q_m$. The extension of our analysis to higher bands of the effective bilayer system might be pursued with a similar localization ansatz [64].

V. CONCLUSION

In this paper, we analytically described the overall optical response of the alternating-twist trilayer system. By performing a unitary transformation that decouples the trilayer Hamiltonian into an effective bilayer and a monolayer Hamiltonian, we showed that the optical response is basically given by the (known) responses of the bilayer and monolayer systems. However, the coupled response of the bilayer and single-layer current densities also appears, and this is proportional to the in-plane magnetic response. This response is usually very weak and we verified this property by an estimate in the magic-angle regime. Our analysis can explain the practical absence of an in-plane orbital magnetic susceptibility in the alternating-twist trilayer graphene [23,24].

We further applied an alternative unitary transformation that involves electric and *local* magnetic moments. In this way, we formulated coupled constitutive equations based on the total electric field and the local magnetic fields. Nevertheless, this magnetoelectric coupling does not lead to optical activity, as no real chirality can persist in this mirror-symmetric setting.

The results in this paper motivate further studies on the electromagnetic response of twisted multilayer systems. In particular, the response of tetralayer systems will be the subject of future studies.

APPENDIX A: ON TIME-REVERSAL SYMMETRY

In this Appendix, we discuss implications of time-reversal symmetry for the surface conductivity. The total electronic Hamiltonian $\mathcal{H}$ of the multilayered system in real space thus satisfies $\mathcal{H} = \mathcal{H}^*$.

We show that a time-reversal ($\mathcal{T}$-) symmetric $\mathcal{H}$ implies a symmetric conductivity matrix, in the sense that interchanging the layer and polarization index pairs leaves the matrix invariant. In particular, we show that (for $\nu, \nu' = x, y$ and $\ell, \ell' = 1, 2, 3$)

$$\sigma_{\nu\nu'}^{\ell\ell'}(\omega) = \sigma_{\nu'\nu}^{\ell'\ell}(\omega), \quad \text{every } \omega \in \mathbb{C}. \quad (A1)$$

To prove Eq. (A1), we start with the fact that there exists an antiunitary transformation $\mathfrak{U}$ such that for each eigenvector $|\psi\rangle$ of $\mathcal{H}$ we have the invariance property $|\psi\rangle = \mathfrak{U}|\psi\rangle$. We apply $\mathfrak{U}^{-1} j_{0\nu}^{\ell} \mathfrak{U} = -j_{0\nu}^{\ell}$, where $j_{0\nu}^{\ell}$ denotes the ν-directed initial current of the lth layer.

The trace of the Kubo formulation yields the following formula for the layer-resolved surface conductivity:

$$\sigma_{\nu\nu'}^{\ell\ell'}(\omega) = -\frac{e^2}{\hbar(\omega + i0^+)} \sum_{\{|\psi\rangle, |\psi'\rangle\}} \frac{f(E_\psi) - f(E_{\psi'})}{i(\omega + i0^+ + \omega_{\psi\psi'})}$$

$$\times \langle\psi|\mathfrak{U}^{-1} j_{0,\nu}^{\ell} \mathfrak{U}|\psi'\rangle^* \langle\psi'|\mathfrak{U}^{-1} j_{0,\nu'}^{\ell'} \mathfrak{U}|\psi\rangle^*$$

$$= -\frac{e^2}{\hbar(\omega + i0^+)} \sum_{\{|\psi\rangle, |\psi'\rangle\}} \frac{f(E_\psi) - f(E_{\psi'})}{i(\omega + i0^+ + \omega_{\psi\psi'})}$$

$$\times \langle\psi|\left(j_{0,\nu'}^{\ell'}\right)^\dagger|\psi'\rangle \langle\psi'|\left(j_{0,\nu}^{\ell}\right)^\dagger|\psi\rangle \quad \text{(real } \omega\text{)}.$$

Here, E_ψ is the energy (eigenvalue of $\mathcal{H}$) corresponding to the normalized eigenvector $|\psi\rangle$ of $\mathcal{H}$, $f(E)$ is the Fermi-Dirac distribution, and $\omega_{\psi\psi'} = (E_\psi - E_{\psi'})/\hbar$. Relation (A1) follows by the Hermiticity of the current. This result can be analytically continued to complex ω.

In our model, the Hamiltonian is given approximately near the K or K' valley. Each of these Hamiltonians is not $\mathcal{T}$ symmetric. Since the total Hamiltonian is $\mathcal{T}$ symmetric, we apply the symmetrization

$$\sigma_{\nu\nu'}^{\ell\ell'}(\omega) = \left[\sigma_{\nu\nu',K}^{\ell\ell'}(\omega) + \sigma_{\nu'\nu,K}^{\ell'\ell}(\omega)\right]/2, \quad (A2)$$

where $\sigma_{\nu\nu',K}^{\ell\ell'}$ is due to the K valley. The resulting conductivity formulas will include the valley degeneracy factor $g_v = 2$ and a spin degeneracy factor $g_s = 2$.

APPENDIX B: HAMILTONIAN OF TRILAYER SYSTEM AND UNITARY TRANSFORMATION TO DIRECT SUM

In this Appendix, we describe the Dirac Hamiltonian of the alternating-twist trilayer system in real space; and transform it unitarily into a direct sum of effective twisted bilayer and single-layer Hamiltonians, following Ref. [53]. Our setting lacks mirror symmetry.

1. Model Hamiltonian and moiré potentials

The electron Schrödinger state vector is of the form

$$\psi = \left(\{\psi_\ell^s\}\right)^T = \left(\psi_1^A \quad \psi_1^B \quad \psi_2^A \quad \psi_2^B \quad \psi_3^A \quad \psi_3^B\right)^T.$$

The twist angle of layer ℓ is $\theta_\ell = (-1)^\ell \theta/2$ ($\ell = 1, 2, 3$). In the sublattice-layer representation, the unperturbed Hamiltonian of the K valley reads as

$$\mathcal{H}_K^{\text{tri}} = \begin{pmatrix} \mathfrak{D}(\theta) & \mathfrak{T}^{12}(\boldsymbol{x}) & 0 \\ \mathfrak{T}^{12}(\boldsymbol{x})^\dagger & \mathfrak{D}(-\theta) & \mathfrak{T}^{23}(\boldsymbol{x}) \\ 0 & \mathfrak{T}^{23}(\boldsymbol{x})^\dagger & \mathfrak{D}(\theta) \end{pmatrix}; \quad (B1)$$

$\boldsymbol{x} = (x, y)^T$ is the position vector in the reference plane ($\boldsymbol{x} \in \mathbb{R}^2$). The matrix-valued Dirac operator is

$$\mathfrak{D}(\theta) = v_F \hbar \begin{pmatrix} 0 & -2ie^{-i\frac{\theta}{2}}\partial \\ -2ie^{i\frac{\theta}{2}}\bar{\partial} & 0 \end{pmatrix}, \quad (B2)$$

where $v_F \simeq 10^6$ m/s is the Fermi velocity of graphene, $\partial = (\partial_x - i\partial_y)/2$, and $\bar{\partial} = (\partial_x + i\partial_y)/2$ in the xy plane.

The related moiré potentials are described by

$$\mathfrak{T}^{\ell\ell'}(\boldsymbol{x}) = \begin{pmatrix} w_{AA}^{\ell\ell'} U_0^{\ell\ell'}(\boldsymbol{x}) & w_{AB}^{\ell\ell'} U_1^{\ell\ell'}(\boldsymbol{x}) \\ w_{AB}^{\ell\ell'} U_1^{\ell\ell'*}(-\boldsymbol{x}) & w_{AA}^{\ell\ell'} U_0^{\ell\ell'}(\boldsymbol{x}) \end{pmatrix} \quad (B3)$$

for $\ell' = \ell + 1$ (if $\ell = 1, 2$), where $w_{AA}^{\ell\ell'} = \kappa w_{AB}^{\ell\ell'}$, $\kappa > 0$, the coefficients $w_{AB}^{\ell\ell'}$ have units of energy and express interlayer tunneling, and

$$U_\xi^{\ell\ell'}(\boldsymbol{x}) = \sum_{n=1}^3 e^{-i\xi(n-1)\phi} e^{-i\boldsymbol{q}_n^{\ell\ell'} \cdot (\boldsymbol{x} - \boldsymbol{D}_{\ell\ell'})} \quad (B4)$$

with $\phi = 2\pi/3$ and $\xi = 0, 1$. Here, we define [53]

$$\boldsymbol{q}_1^{\ell\ell'} = 2k_D \sin\left(\frac{\theta_{\ell'\ell}}{2}\right) \mathcal{R}_{\phi_{\ell\ell'}} \cdot (0, -1)^T, \quad (B5)$$

$$\boldsymbol{q}_{2,3}^{\ell\ell'} = \mathcal{R}_{\pm\phi} \boldsymbol{q}_1^{\ell\ell'}, \quad (B6)$$

$$\boldsymbol{D}_{\ell\ell'} = \frac{\boldsymbol{d}_\ell + \boldsymbol{d}_{\ell'}}{2} + i \cot\left(\frac{\theta_{\ell'\ell}}{2}\right) \boldsymbol{\tau}_y \cdot \frac{\boldsymbol{d}_\ell - \boldsymbol{d}_{\ell'}}{2}, \quad (B7)$$

$$\theta_{\ell'\ell} = \theta_{\ell'} - \theta_\ell, \quad \phi_{\ell\ell'} = \frac{\theta_\ell + \theta_{\ell'}}{2},$$

$$\mathcal{R}_\phi = \begin{pmatrix} \cos\phi & -\sin\phi \\ \sin\phi & \cos\phi \end{pmatrix}, \quad (B8)$$

where $k_D = |\boldsymbol{K}| = 4\pi/(3\sqrt{3}a_C)$ is the Dirac momentum, $\boldsymbol{\tau}_y$ is the y-Pauli matrix, and $a_C \simeq 1.42$ Å is the carbon-carbon distance. The vector $\boldsymbol{d}_\ell$ is the lateral shift of the ℓth layer, and $\boldsymbol{D}_{\ell\ell'}$ amounts to shifts in the potentials. We set $\boldsymbol{d}_\ell = \boldsymbol{d} = (d_1, d_2)^T$ for all ℓ by which $\boldsymbol{D}_{\ell\ell'} = \boldsymbol{d}$.

Next, we nondimensionalize the model via the mapping $\boldsymbol{x} \mapsto \check{\boldsymbol{x}} = 2k_D \sin(\theta/2)\boldsymbol{x}$ [53]. Let the scaled position and shift vectors be $\check{\boldsymbol{x}}$ and $\check{\boldsymbol{d}}$. The Hamiltonian $\mathcal{H}_K^{\text{tri}}$ exhibits the energy scale $2v_F \hbar k_D \sin(\theta/2)$; $\mathcal{H}_K^{\text{tri}} \mapsto \check{\mathcal{H}}_K^{\text{tri}} = [2v_F \hbar k_D \sin(\theta/2)]^{-1} \mathcal{H}_K^{\text{tri}}$. We define

$$\alpha_{\ell\ell'} = \frac{w_{AB}^{\ell\ell'}}{2v_F \hbar k_D \sin(\theta/2)} > 0, \quad \ell' = \ell + 1 \, (\ell = 1, 2).$$

For ease of notation, we remove the breve symbol from $\check{\boldsymbol{x}}, \check{\boldsymbol{d}}$, and $\check{\mathcal{H}}_K^{\text{tri}}$, thus using $\boldsymbol{x}, \boldsymbol{d} = (d_1, d_2)^T$ and $\mathcal{H}_K^{\text{tri}}$ as the moiré-scaled variables; ditto for the potentials $\mathfrak{T}^{\ell\ell'}$.

Hence, we now have the dimensionless potentials

$$\mathfrak{T}^{12}(\boldsymbol{x}) = \begin{pmatrix} \kappa\alpha_{12}U_0(\boldsymbol{x}) & \alpha_{12}U_1^*(-\boldsymbol{x}) \\ \alpha_{12}U_1(\boldsymbol{x}) & \kappa\alpha_{12}U_0(\boldsymbol{x}) \end{pmatrix},$$

$$\mathfrak{T}^{23}(\boldsymbol{x}) \simeq \begin{pmatrix} \kappa\alpha_{23}U_0^*(\boldsymbol{x}) & \alpha_{23}U_1^*(\boldsymbol{x}) \\ \alpha_{23}U_1(-\boldsymbol{x}) & \kappa\alpha_{23}U_0^*(\boldsymbol{x}) \end{pmatrix}.$$

If $\alpha_{12} \neq \alpha_{23}$ the ensuing Hamiltonian may lack mirror symmetry. This symmetry is recovered if $\alpha_{12} = \alpha_{23}$.

In view of $|\boldsymbol{d}| \ll 1$, we have set

$$U_0(\boldsymbol{x}) = U_0^{12}(\boldsymbol{x}), \quad U_0^{12*}(\boldsymbol{x}) = U_0^*(\boldsymbol{x}),$$

$$U_0^{23}(\boldsymbol{x}) = U_0^*(\boldsymbol{x}), \quad U_0^{23*}(\boldsymbol{x}) = U_0(\boldsymbol{x}),$$

$$U_1(\boldsymbol{x}) = U_1^{12*}(-\boldsymbol{x}), \quad U_1^{12}(\boldsymbol{x}) = U_1^*(-\boldsymbol{x}),$$

$$U_1^{23}(\boldsymbol{x}) \simeq U_1^*(\boldsymbol{x}), \quad U_1^{23*}(-\boldsymbol{x}) \simeq U_1(-\boldsymbol{x}).$$

In the above, the first and fifth equations introduce U_0 and U_1, while the last two equations are implied by the condition $|\boldsymbol{d}| \ll 1$.

For the sake of clarity, we give the explicit formulas for U_0 and U_1 at the moiré scale. These are

$$U_0(\boldsymbol{x}) = e^{i(y-d_2)} + e^{-i(\frac{\sqrt{3}}{2}(x-d_1)+\frac{1}{2}(y-d_2))}$$

$$+ e^{-i(-\frac{\sqrt{3}}{2}(x-d_1)+\frac{1}{2}(y-d_2))}$$

$$\simeq e^{iy} + e^{-i(\frac{\sqrt{3}}{2}x+\frac{1}{2}y)} + e^{-i(-\frac{\sqrt{3}}{2}x+\frac{1}{2}y)}, \quad \text{(B9)}$$

$$U_1(\boldsymbol{x}) \simeq e^{iy} + e^{i\frac{2\pi}{3}}e^{-i(\frac{\sqrt{3}}{2}x+\frac{1}{2}y)} + e^{-i\frac{2\pi}{3}}e^{-i(-\frac{\sqrt{3}}{2}x+\frac{1}{2}y)}. \quad \text{(B10)}$$

The Hamiltonian $\mathcal{H}^{\mathrm{tri}}_{K'}$ of the K' valley comes from the complex conjugation of $\mathcal{H}^{\mathrm{tri}}_K$ above. Thus, we write

$$\mathcal{H}^{\mathrm{tri}}_{K'} = \left(\mathcal{H}^{\mathrm{tri}}_K\right)^*$$

in real space. Thus, the eigenvector (basis) sets of the two Hamiltonians are related by an antiunitary transformation. The total contribution to the conductivity from both valleys under time-reversal symmetry in linear response can be extracted from the K-valley Hamiltonian by a simple transposition. One must then symmetrize the optical conductivity (Appendix A).

2. Unitary transformations and direct sum

Next, we outline the steps of a unitary transformation on $\mathcal{H}^{\mathrm{tri}}_K$, which eventually yields the mapping

$$\mathcal{H}^{\mathrm{tri}}_K \mapsto \mathcal{H}^{\mathrm{eff}}_K = \mathfrak{S}^\dagger \mathcal{H}^{\mathrm{tri}}_K \mathfrak{S} = \mathcal{H}^{(2)}_{\lambda,K} \oplus \mathcal{H}^{(1)}_K, \quad \text{(B11)}$$

where $\mathcal{H}^{(2)}_{\lambda,K}$ is the effective, K-valley twisted bilayer Hamiltonian with parameter $\lambda = \sqrt{\alpha_{12}^2 + \alpha_{23}^2}$, and $\mathcal{H}^{(1)}_K$ is the respective single-layer Hamiltonian, as explained below. Hence, we can write any eigenvector of $\mathcal{H}^{\mathrm{eff}}_K$ in the form $(|b\rangle_1, |b\rangle_2, 0)^T$ or $(0, 0, |s\rangle)^T$ where $(|b\rangle_1, |b\rangle_2)^T$ and $|s\rangle$ are eigenvectors of $\mathcal{H}^{(2)}_{\lambda,K}$ and $\mathcal{H}^{(1)}_K$, respectively. We have

$$\mathcal{H}^{(2)}_{\lambda,K}\begin{pmatrix} |b\rangle_1 \\ |b\rangle_2 \end{pmatrix} = E_b^{(2)}\begin{pmatrix} |b\rangle_1 \\ |b\rangle_2 \end{pmatrix}, \quad \mathcal{H}^{(1)}_K|s\rangle = E_s^{(1)}|s\rangle;$$

$E_{b,s}^{(2,1)}$ is the eigenvalue of the Dirac Hamiltonian for the twisted bilayer (b) and single-layer (s) system. Each of the symbols s and b stands for the combined band index and continuum quasimomentum variable of the scaled Brillouin zone. We set $E_s = E_s^{(1)}$ and $E_b = E_b^{(2)}$.

We will show that in the sublattice-layer form [53]

$$\mathfrak{S} = \begin{pmatrix} \alpha_{12}/\lambda & 0 & \alpha_{23}/\lambda \\ 0 & 1 & 0 \\ \alpha_{23}/\lambda & 0 & -\alpha_{12}/\lambda \end{pmatrix}. \quad \text{(B12)}$$

Note that $\mathfrak{S}$ is represented by a 6×6 matrix. In the case with mirror symmetry, if $\alpha_{12} = \alpha_{23}$, we have

$$\mathfrak{S} = \frac{1}{\sqrt{2}}\begin{pmatrix} 1 & 0 & 1 \\ 0 & \sqrt{2} & 0 \\ 1 & 0 & -1 \end{pmatrix}. \quad \text{(B13)}$$

This unitary transformation is described as a result of four basic, successive unitary operations, as detailed below [53]. To simplify notation, we will omit the valley index (K), unless we state otherwise.

a. Layer ordering

We apply $\mathcal{H}^{\mathrm{tri}} \mapsto \mathring{\mathcal{H}} := \Omega^\dagger \mathcal{H}^{\mathrm{tri}} \Omega$ with state vector

$$\psi = \begin{pmatrix} \psi_1^A & \psi_1^B & \psi_2^A & \psi_2^B & \psi_3^A & \psi_3^B \end{pmatrix}^T$$

$$\mapsto \mathring{\psi} = \Omega^\dagger \psi = \begin{pmatrix} \psi_1^A & \psi_2^A & \psi_3^A & \psi_1^B & \psi_2^B & \psi_3^B \end{pmatrix}^T.$$

The transformation operator Ω in matrix form is

$$\Omega = \begin{pmatrix} 1 & 0 & 0 & 0 & 0 & 0 \\ 0 & 0 & 0 & 1 & 0 & 0 \\ 0 & 1 & 0 & 0 & 0 & 0 \\ 0 & 0 & 0 & 0 & 1 & 0 \\ 0 & 0 & 1 & 0 & 0 & 0 \\ 0 & 0 & 0 & 0 & 0 & 1 \end{pmatrix}.$$

b. Layer alignment

We now apply $\mathring{\mathcal{H}} \mapsto \check{\mathcal{H}} = Y^\dagger \mathring{\mathcal{H}} Y$ so that

$$\mathring{\psi} = \begin{pmatrix} \psi_1^A & \psi_2^A & \psi_3^A & \psi_1^B & \psi_2^B & \psi_3^B \end{pmatrix}^T$$

$$\mapsto \check{\psi} = Y^\dagger \mathring{\psi} = \begin{pmatrix} \psi_1^A & \psi_3^A & \psi_2^A & \psi_1^B & \psi_3^B & \psi_2^B \end{pmatrix}^T;$$

$$Y = \begin{pmatrix} 1 & 0 & 0 & 0 & 0 & 0 \\ 0 & 0 & 1 & 0 & 0 & 0 \\ 0 & 1 & 0 & 0 & 0 & 0 \\ 0 & 0 & 0 & 1 & 0 & 0 \\ 0 & 0 & 0 & 0 & 0 & 1 \\ 0 & 0 & 0 & 0 & 1 & 0 \end{pmatrix}.$$

Thus, we have [53]

$$\check{\mathcal{H}} = \begin{pmatrix} \mathcal{M} & \mathcal{D}^\dagger \\ \mathcal{D} & \mathcal{M} \end{pmatrix},$$

$$\mathcal{M} = \kappa \begin{pmatrix} 0 & 0 & \alpha_{12}U_0(\boldsymbol{x}) \\ 0 & 0 & \alpha_{23}U_0(\boldsymbol{x}) \\ \alpha_{12}U_0^*(\boldsymbol{x}) & \alpha_{23}U_0^*(\boldsymbol{x}) & 0 \end{pmatrix}$$

$$= \kappa \begin{pmatrix} \mathbf{0} & WU_0(\boldsymbol{x}) \\ W^T U_0^*(\boldsymbol{x}) & 0 \end{pmatrix}, \quad W = \begin{pmatrix} \alpha_{12} \\ \alpha_{23} \end{pmatrix}.$$

Here, $\mathcal{D}$ is represented by the following 3×3 matrix:

$$\mathcal{D} = \begin{pmatrix} -2ie^{i\theta/2}\bar{\partial} & WU_1(\boldsymbol{x}) \\ W^T U_1(-\boldsymbol{x}) & -2ie^{-i\theta/2}\bar{\partial} \end{pmatrix}.$$

$$\widehat{\mathcal{H}} = \begin{pmatrix} 0 & 0 & \kappa\lambda U_0(\boldsymbol{x}) & -2ie^{-i\theta/2}\partial & 0 & \lambda U_1^*(-\boldsymbol{x}) \\ 0 & 0 & 0 & 0 & -2ie^{-i\theta/2}\partial & 0 \\ \kappa\lambda U_0^*(\boldsymbol{x}) & 0 & 0 & \lambda U_1^*(\boldsymbol{x}) & 0 & -2ie^{i\theta/2}\partial \\ -2ie^{i\theta/2}\bar{\partial} & 0 & \lambda U_1(\boldsymbol{x}) & 0 & 0 & \kappa\lambda U_0(\boldsymbol{x}) \\ 0 & -2ie^{i\theta/2}\bar{\partial} & 0 & 0 & 0 & 0 \\ \lambda U_1(-\boldsymbol{x}) & 0 & -2ie^{-i\theta/2}\bar{\partial} & \kappa\lambda U_0^*(\boldsymbol{x}) & 0 & 0 \end{pmatrix}.$$

d. Conversion to direct sum

We apply $\widehat{\mathcal{H}} \mapsto \mathcal{H}^{\text{eff}} = Z^\dagger \widehat{\mathcal{H}} Z = \mathcal{H}_\lambda^{(2)} \oplus \mathcal{H}^{(1)}$ with

$$Z = \begin{pmatrix} 1 & 0 & 0 & 0 & 0 & 0 \\ 0 & 0 & 0 & 0 & 1 & 0 \\ 0 & 0 & 1 & 0 & 0 & 0 \\ 0 & 1 & 0 & 0 & 0 & 0 \\ 0 & 0 & 0 & 0 & 0 & 1 \\ 0 & 0 & 0 & 1 & 0 & 0 \end{pmatrix}.$$

In the above, $\mathcal{H}^{(1)}$ and $\mathcal{H}_\lambda^{(2)}$ denote the moiré-scaled effective single-layer and twisted bilayer Hamiltonians, respectively. To simplify notation, set $\mathcal{H}^{(1)} = \mathcal{H}_1$ and $\mathcal{H}_\lambda^{(2)} = \mathcal{H}_2$. These operators read as

$$\mathcal{H}_1 = \mathfrak{D}(\theta) = \begin{pmatrix} 0 & -2ie^{-i\theta/2}\partial \\ -2ie^{i\theta/2}\bar{\partial} & 0 \end{pmatrix} \tag{B14}$$

and

$$\mathcal{H}_2 = \begin{pmatrix} \mathfrak{D}(\theta) & \lambda\mathcal{U}(\boldsymbol{x}) \\ \lambda\mathcal{U}(\boldsymbol{x})^\dagger & \mathfrak{D}(-\theta) \end{pmatrix}, \tag{B15}$$

where

$$\mathcal{U}(\boldsymbol{x}) = \begin{pmatrix} \kappa U_0(\boldsymbol{x}) & U_1^*(-\boldsymbol{x}) \\ U_1(\boldsymbol{x}) & \kappa U_0(\boldsymbol{x}) \end{pmatrix}.$$

In summary, the operator $\mathfrak{S}$ of Eq. (B12), which converts the K-valley Hamiltonian $\mathcal{H}_K^{\text{tri}}$ to $\mathcal{H}_K^{\text{eff}}$, is computed directly by $\mathfrak{S} = \Omega Y V Z$. The corresponding matrix is real. Hence, the same matrix is used to convert the K'-valley Hamiltonian, $\mathcal{H}_{K'}^{\text{tri}} = (\mathcal{H}_K^{\text{tri}})^*$ in real space, into a direct sum of effective twisted bilayer and single-layer Hamiltonians.

c. Singular-value decomposition

Next, we apply $\check{\mathcal{H}} \mapsto \widehat{\mathcal{H}} = V^\dagger \check{\mathcal{H}} V$ where

$$V = \begin{pmatrix} \mathcal{V} & 0 \\ 0 & \mathcal{V} \end{pmatrix}, \quad \mathcal{V} = \text{diag}(\mathcal{A}, \mathcal{B}),$$

and the 2×2 matrix $\mathcal{A}$ and scalar $\mathcal{B}$ stem from $W = \mathcal{A}\Lambda\mathcal{B}^*$ with $\Lambda = (\lambda, 0)^T$ and $\lambda = \sqrt{W^T W} = \sqrt{\alpha_{12}^2 + \alpha_{23}^2}$. By a direct computation, we have

$$\mathcal{A} = \begin{pmatrix} \alpha_{12}/\lambda & \alpha_{23}/\lambda \\ \alpha_{23}/\lambda & -\alpha_{12}/\lambda \end{pmatrix}, \quad \mathcal{B} = 1.$$

The transformed Hamiltonian is thus written as

APPENDIX C: OPTICAL CONDUCTIVITY OF ALTERNATING-TWIST TRILAYER SYSTEM: CALCULATIONS

In this Appendix, we determine the optical conductivity for the alternating-twist trilayer system by the Kubo formulation without mirror symmetry. The main assumptions are time-reversal symmetry and spatial isotropy. We invoke the unitary transformation of the K-valley trilayer Hamiltonian into a direct sum of the effective Hamiltonians $\mathcal{H}_1$ and $\mathcal{H}_2$ (Appendix B). We use moiré-scaled quantities, so that the units of length and energy are $\{2k_D \sin(\theta/2)\}^{-1}$ and $2v_F \hbar k_D \sin(\theta/2)$. Thus, the (dimensionless) current operator in layer ℓ is $\boldsymbol{j}^\ell = -i[\boldsymbol{x}^\ell, \mathcal{H}^{\text{tri}}]$, where $\mathcal{H}^{\text{tri}}$ and $\boldsymbol{x}^\ell$ are the moiré-scaled trilayer Hamiltonian and vector position. We often suppress the subscript K for the valley.

1. Methodology and general results

We transform the unperturbed trilayer Hamiltonian $\mathcal{H}_K^{\text{tri}}$, by $\mathfrak{S}$ into the direct sum $\mathcal{H}_2 \oplus \mathcal{H}_1$. Hence, we compute the trace of the current-current commutators on the basis formed by the eigenvectors of $\mathcal{H}_2 \oplus \mathcal{H}_1$. Consider the set of all state vectors of the form

$$|\underline{\psi}\rangle = \mathfrak{S}^\dagger |\psi\rangle = \begin{pmatrix} |b\rangle_1 \\ |b\rangle_2 \\ 0 \end{pmatrix} \text{ or } \begin{pmatrix} 0 \\ 0 \\ |s\rangle \end{pmatrix},$$

which are eigenvectors of $\mathcal{H}_2 \oplus \mathcal{H}_1$; $|b\rangle = (|b\rangle_1, |b\rangle_2)^T$ and $|s\rangle$ denote the effective twisted bilayer and single-layer Hamiltonian eigenvectors, with energies $E_b = E_b^{(2)}$ and $E_s = E_s^{(1)}$. The symbols b and s express the combined band index and quasimomentum in the scaled moiré Brillouin zone.

For real ω, the K-valley Kubo formula yields

$$\sigma_{\nu\nu',K}^{\ell\ell'}(\omega) = C_0 \frac{e^2}{\hbar(\omega + i\delta)} \sum_{\{|\underline{\psi}\rangle\}} f(E_\psi) \int_0^\infty dt \, e^{i(\omega+i\delta)t} \langle \underline{\psi}|[\underline{j}_{\nu,K}^\ell(t), \underline{j}_{\nu',K}^{\ell'}(0)]|\underline{\psi}\rangle$$

$$= C_0 \frac{e^2}{\hbar(\omega + i\delta)} \left\{ \sum_b f_b \int_0^\infty dt \, e^{i(\omega+i\delta)t} (_1\langle b|, _2\langle b|) \left(V_{bb,\nu\nu'}^{\ell\ell'}(t) - V_{bb,\nu\nu'}^{\ell\ell'}(t)^\dagger\right) \begin{pmatrix} |b\rangle_1 \\ |b\rangle_2 \end{pmatrix} \right.$$

$$\left. + \sum_s f_s \int_0^\infty dt \, e^{i(\omega+i\delta)t} \times \langle s|V_{ss,\nu\nu'}^{\ell\ell'}(t) - V_{ss,\nu\nu'}^{\ell\ell'}(t)^\dagger|s\rangle \right\}, \quad \delta \downarrow 0, \quad (C1)$$

for $\ell, \ell' = 1, 2, 3$ and $\nu, \nu' = x, y$. The ν-directed current $\underline{j}_{\nu,K}^\ell(t) = \mathfrak{S}^\dagger j_{\nu,K}^\ell(t)\mathfrak{S}$, frequency ω and time t are moiré scaled and dimensionless; and $C_0 = \{4k_D^2 \sin^2(\theta/2)A_m\}^{-1} = \frac{3\sqrt{3}}{8\pi^2}$ where $A_m = \frac{3\sqrt{3}}{8}(\frac{a_C}{\sin(\theta/2)})^2$ is the area of the moiré cell and a_C is the carbon-carbon distance. We set $f_\eta = f(E_\eta)$ as the Fermi-Dirac distribution, and $V_{\eta\eta',\nu\nu'}^{\ell\ell'}(t) = \mathbf{e}_\nu \cdot \mathbf{V}_{\eta\eta'}^{\ell\ell'}(t) \cdot \mathbf{e}_{\nu'}$ ($\mathbf{e}_\nu$: Cartesian unit vector) for $\eta, \eta' = b, s$. The matrix-valued operator $\mathbf{V}_{\eta\eta'}^{\ell\ell'}(t)$ is defined by

$$\underline{j}_K^\ell(t)\underline{j}_{0,K}^{\ell'} = \begin{pmatrix} \mathbf{V}_{bb}^{\ell\ell'}(t) & \mathbf{V}_{bs}^{\ell\ell'}(t) \\ \mathbf{V}_{sb}^{\ell\ell'}(t) & \mathbf{V}_{ss}^{\ell\ell'}(t) \end{pmatrix}, \quad (C2)$$

and thus vanishes for $t < 0$; $\underline{j}_0^\ell = \underline{j}^\ell(0)$. By Eq. (C1), we only need the diagonal terms $\mathbf{V}_{\eta\eta}^{\ell\ell'}(t)$. The symbol $\sum_\eta$ ($\eta = b, s$) means summation over band indices and integration in the quasimomentum over the scaled Brillouin zone. The elements $\langle\eta| \cdot |\eta\rangle$ ($\eta = b, s$) of Eq. (C1) account for x-inner products of scalar Bloch wave functions, which compose $\langle\mathbf{x}|\eta\rangle$.

In Eq. (C1), each sum $\sum_\eta$ is replaced by $\sum_{\eta,\eta'}$ or $\sum_{\eta,\bar{\eta}'}$ by use of the resolution of the identity $1 = \sum_\eta |\eta\rangle\langle\eta|$ in the respective Hilbert space (for $\eta = b, s$). Here, we set $(\eta, \eta') = (b, b')$ or (s, s'), while $\bar{\eta}'$ in $(\eta, \bar{\eta}')$ takes values complementary to those of η in the sense that $\bar{\eta}' = s'$ if $\eta = b$ and $\bar{\eta}' = b'$ if $\eta = s$.

For every η in these sums, the Fourier transform of $\langle\eta|V_{\eta\eta,\nu\nu'}^{\ell\ell'}(t)|\eta\rangle$ contributes the factors

$$-\frac{1}{i(\omega + \omega_{\eta\eta'} + i\delta)} \quad \text{or} \quad -\frac{1}{i(\omega + \omega_{\eta\bar{\eta}'} + i\delta)},$$

as $\delta \downarrow 0$. The Fourier transform of $\langle\eta|V_{\eta\eta,\nu\nu'}^{\ell\ell'}(t)^\dagger|\eta\rangle$ contributes the respective factors

$$-\frac{1}{i(\omega - \omega_{\eta\eta'} + i\delta)} \quad \text{or} \quad -\frac{1}{i(\omega - \omega_{\eta\bar{\eta}'} + i\delta)}.$$

The ensuing optical conductivity tensor $\boldsymbol{\sigma}(\omega)$ comes from the symmetrization of the K-valley contribution (Appendix A). This tensor $\boldsymbol{\sigma}$ reads as

$$\boldsymbol{\sigma}(\omega) = \begin{pmatrix} \boldsymbol{\sigma}^{11}(\omega) & \boldsymbol{\sigma}^{12}(\omega) & \boldsymbol{\sigma}^{13}(\omega) \\ \boldsymbol{\sigma}^{21}(\omega) & \boldsymbol{\sigma}^{22}(\omega) & \boldsymbol{\sigma}^{23}(\omega) \\ \boldsymbol{\sigma}^{31}(\omega) & \boldsymbol{\sigma}^{32}(\omega) & \boldsymbol{\sigma}^{33}(\omega) \end{pmatrix},$$

where $\boldsymbol{\sigma}^{\ell\ell'}$ are 2×2 matrices for the layer-resolved conductivities. We will express $\boldsymbol{\sigma}^{\ell\ell'}$ in terms of principal conductivities associated with two effective, simpler systems, for *arbitrary*

positive parameters $\alpha_{12(23)}$ of the trilayer Hamiltonian $\mathcal{H}_K^{\text{tri}}$ (Appendix B).

After some algebra, we obtain (see Appendix C 3)

$$\boldsymbol{\sigma}^{11} = \lambda^{-4}\left(\alpha_{12}^4 \boldsymbol{\sigma}_{\text{BL}}^{11} + \alpha_{23}^4 \boldsymbol{\sigma}_{\text{SL}} + \alpha_{12}^2\alpha_{23}^2 \boldsymbol{\sigma}_c\right) \quad (C3)$$

$$= \begin{pmatrix} \sigma_0^{11} & 0 \\ 0 & \sigma_0^{11} \end{pmatrix}, \quad (C4)$$

$$\boldsymbol{\sigma}^{12} = \frac{\alpha_{12}^2}{\lambda^2} \boldsymbol{\sigma}_{\text{BL}}^{12}$$

$$= \begin{pmatrix} \sigma_0^{12} & \sigma_{xy}^{12} \\ -\sigma_{xy}^{12} & \sigma_0^{12} \end{pmatrix} = (\boldsymbol{\sigma}^{21})^T, \quad (C5)$$

$$\boldsymbol{\sigma}^{13} = \frac{\alpha_{12}^2\alpha_{23}^2}{\lambda^4}\left(\boldsymbol{\sigma}_{\text{BL}}^{11} + \boldsymbol{\sigma}_{\text{SL}} - \boldsymbol{\sigma}_c\right) \quad (C6)$$

$$= \begin{pmatrix} \sigma_0^{13} & 0 \\ 0 & \sigma_0^{13} \end{pmatrix} = \boldsymbol{\sigma}^{31}, \quad (C7)$$

$$\boldsymbol{\sigma}^{22} = \boldsymbol{\sigma}_{\text{BL}}^{22} = \begin{pmatrix} \sigma_0^{22} & 0 \\ 0 & \sigma_0^{22} \end{pmatrix}, \quad (C8)$$

$$\boldsymbol{\sigma}^{23} = \frac{\alpha_{23}^2}{\lambda^2} \boldsymbol{\sigma}_{\text{BL}}^{21}$$

$$= \frac{\alpha_{23}^2}{\alpha_{12}^2} \boldsymbol{\sigma}^{21} = (\boldsymbol{\sigma}^{32})^T, \quad (C9)$$

$$\boldsymbol{\sigma}^{33} = \lambda^{-4}\left(\alpha_{23}^4 \boldsymbol{\sigma}_{\text{BL}}^{11} + \alpha_{12}^4 \boldsymbol{\sigma}_{\text{SL}} + \alpha_{12}^2\alpha_{23}^2 \boldsymbol{\sigma}_c\right)$$

$$= \boldsymbol{\sigma}^{11}|_{\alpha_{12}\leftrightarrow\alpha_{23}} = \begin{pmatrix} \sigma_0^{33} & 0 \\ 0 & \sigma_0^{33} \end{pmatrix}. \quad (C10)$$

The first equation for $\boldsymbol{\sigma}^{33}$ comes from interchanging the constants α_{12} and α_{23} in $\boldsymbol{\sigma}^{11}$. In Eqs. (C3)–(C10), we express the layer-resolved conductivities in terms of the principal 2×2 matrices $\boldsymbol{\sigma}_{\text{BL}}^{\varsigma\varsigma'}$, $\boldsymbol{\sigma}_{\text{SL}}$, and $\boldsymbol{\sigma}_c$ ($\varsigma, \varsigma' = 1, 2$). Here, $\boldsymbol{\sigma}_{\text{BL}}^{\varsigma\varsigma'}$ and $\boldsymbol{\sigma}_{\text{SL}}$ are conductivities that separately arise from the effective twisted bilayer and single-layer Hamiltonians, respectively [cf. Eqs. (B15) and (B14) in Appendix B]. On the other hand, $\boldsymbol{\sigma}_c$ couples the two effective systems.

The principal matrices have the forms

$$\boldsymbol{\sigma}_{\text{SL}} = \begin{pmatrix} \sigma_e^{(1)} & 0 \\ 0 & \sigma_e^{(1)} \end{pmatrix},$$

$$\boldsymbol{\sigma}_{\text{BL}}^{\varsigma\varsigma} = \begin{pmatrix} \sigma_e^{(2)} & 0 \\ 0 & \sigma_e^{(2)} \end{pmatrix} \quad (\varsigma = 1, 2),$$

$$\boldsymbol{\sigma}_{\text{BL}}^{12} = \begin{pmatrix} \sigma_e^{12} & \sigma_{e,xy}^{12} \\ -\sigma_{e,xy}^{12} & \sigma_e^{12} \end{pmatrix} = \left(\boldsymbol{\sigma}_{\text{BL}}^{21}\right)^T,$$

$$\boldsymbol{\sigma}_c = \begin{pmatrix} \sigma_c & 0 \\ 0 & \sigma_c \end{pmatrix}.$$

The scalars $\sigma_e^{(1,2)}$, σ_e^{12}, $\sigma_{e,xy}^{12}$, and σ_c, respectively, denote the in-plane conductivities of the effective single-layer and twisted bilayer systems, the covalent drag and chiral (or Hall) conductivities of the effective bilayer system, and the coupling of the two systems. Note that $\sigma_0^{22} = \sigma_e^{(2)}$ in Eq. (C8). In Appendix C 3, we express all these scalar functions of ω in terms of inner products of suitable pseudo-spin-wave functions.

Hence, the elements $\sigma_0^{\ell\ell'}$ of Eqs. (C3)–(C10) are

$$\sigma_0^{11} = \lambda^{-4}\left(\alpha_{12}^4 \sigma_e^{(2)} + \alpha_{23}^4 \sigma_e^{(1)} + \alpha_{12}^2 \alpha_{23}^2 \sigma_c\right), \tag{C11}$$

$$\sigma_0^{12} = \frac{\alpha_{12}^2}{\lambda^2}\sigma_e^{12}, \quad \sigma_{xy}^{12} = \frac{\alpha_{12}^2}{\lambda^2}\sigma_{e,xy}^{12}, \tag{C12}$$

$$\sigma_0^{13} = \frac{\alpha_{12}^2 \alpha_{23}^2}{\lambda^4}\left(\sigma_e^{(2)} + \sigma_e^{(1)} - \sigma_c\right), \tag{C13}$$

$$\sigma_0^{22} = \sigma_e^{(2)}, \tag{C14}$$

$$\sigma_0^{33} = \lambda^{-4}\left(\alpha_{23}^4 \sigma_e^{(2)} + \alpha_{12}^4 \sigma_e^{(1)} + \alpha_{23}^2 \alpha_{12}^2 \sigma_c\right)$$
$$= \sigma_0^{11}|_{\alpha_{12}\leftrightarrow\alpha_{23}}. \tag{C15}$$

In particular, let us consider $\alpha_{12} = \alpha_{23}$, by which mirror symmetry is recovered. We find

$$\boldsymbol{\sigma}^{11} = \tfrac{1}{4}\left(\boldsymbol{\sigma}_{\text{BL}}^{11} + \boldsymbol{\sigma}_{\text{SL}} + \boldsymbol{\sigma}_c\right), \tag{C16}$$

$$\boldsymbol{\sigma}^{12} = \tfrac{1}{2}\boldsymbol{\sigma}_{\text{BL}}^{12} = \left(\boldsymbol{\sigma}^{21}\right)^T, \tag{C17}$$

$$\boldsymbol{\sigma}^{13} = \tfrac{1}{4}\left(\boldsymbol{\sigma}_{\text{BL}}^{11} + \boldsymbol{\sigma}_{\text{SL}} - \boldsymbol{\sigma}_c\right) = \boldsymbol{\sigma}^{31}, \tag{C18}$$

$$\boldsymbol{\sigma}^{23} = \tfrac{1}{2}\boldsymbol{\sigma}_{\text{BL}}^{21} = \boldsymbol{\sigma}^{21} = \left(\boldsymbol{\sigma}^{32}\right)^T, \tag{C19}$$

$$\boldsymbol{\sigma}^{33} = \boldsymbol{\sigma}^{11}. \tag{C20}$$

2. Trace algebra

Next, we provide details on the layer-resolved conductivities. We compute the unitarily transformed currents and $V_{\eta\eta'}^{\ell\ell'}(t)$ in view of Eq. (B11) of Appendix B and time evolution under Hamiltonian $\mathcal{H}_K^{\text{eff}}$. The trace of the Kubo formula is computed on the basis formed by the eigenvectors of $\mathcal{H}^{\text{eff}} = \mathcal{H}_2 \oplus \mathcal{H}_1$. The unitarily transformed currents are

$$\underline{j}_{0\nu}^{\ell} = \mathfrak{S}^\dagger j_{0\nu}^{\ell} \mathfrak{S}, \quad \underline{j}_{\nu}^{\ell}(t) = e^{i\mathcal{H}^{\text{eff}}t} \underline{j}_{0\nu}^{\ell} e^{-i\mathcal{H}^{\text{eff}}t}.$$

The initial original (nontransformed) ν-directed current in layer ℓ is $j_{0\nu}^{\ell} = \boldsymbol{j}_0^{\ell} \cdot \mathbf{e}_\nu$ with $\boldsymbol{j}_0^{\ell} = -i[\boldsymbol{x}^{\ell}, \mathcal{H}^{\text{tri}}]$, where $\mathbf{e}_\nu$ is a Cartesian unit vector in the xy plane.

Therefore, we start with the matrix representations

$$\boldsymbol{j}_0^1 = \begin{pmatrix} \boldsymbol{\tau}^{-\theta} & 0 & 0 \\ 0 & 0 & 0 \\ 0 & 0 & 0 \end{pmatrix}, \quad \boldsymbol{j}_0^2 = \begin{pmatrix} 0 & 0 & 0 \\ 0 & \boldsymbol{\tau}^{\theta} & 0 \\ 0 & 0 & 0 \end{pmatrix},$$

$$\boldsymbol{j}_0^3 = \begin{pmatrix} 0 & 0 & 0 \\ 0 & 0 & 0 \\ 0 & 0 & \boldsymbol{\tau}^{-\theta} \end{pmatrix}.$$

We have defined

$$\boldsymbol{\tau}^\theta = e^{(i/4)\theta\tau_z}\boldsymbol{\tau}e^{-(i/4)\theta\tau_z}, \quad \boldsymbol{\tau} = \tau_x\mathbf{e}_x + \tau_y\mathbf{e}_y,$$

where τ_ν is the ν-Pauli matrix.

We need to compute

$$\underline{\boldsymbol{j}}^{\ell}(t) = \begin{pmatrix} e^{i\mathcal{H}_2t} & 0 \\ 0 & e^{i\mathcal{H}_1t} \end{pmatrix} \underline{\boldsymbol{j}}_0^{\ell} \begin{pmatrix} e^{-i\mathcal{H}_2t} & 0 \\ 0 & e^{-i\mathcal{H}_1t} \end{pmatrix}$$

in the matrix representation $|L\rangle\langle L'|$, where each of $|L\rangle$ and $|L'\rangle$ is $(|b\rangle_1, |b\rangle_2, 0)^T$ or $(0, 0, |s\rangle)^T$ ($\ell = 1, 2, 3$). For the initial $\mathfrak{S}$-transformed currents, we find

$$\underline{\boldsymbol{j}}_0^1 = \begin{pmatrix} \frac{\alpha_{12}^2}{\lambda^2}\boldsymbol{\tau}_1 & \frac{\alpha_{12}\alpha_{23}}{\lambda^2}\boldsymbol{\tau}_c \\ \frac{\alpha_{12}\alpha_{23}}{\lambda^2}\boldsymbol{\tau}_c^\dagger & \left(\frac{\alpha_{23}}{\lambda}\right)^2\boldsymbol{\tau}^{-\theta} \end{pmatrix}$$
$$= \frac{1}{2}\begin{pmatrix} \boldsymbol{\tau}_1 & \boldsymbol{\tau}_c \\ \boldsymbol{\tau}_c^\dagger & \boldsymbol{\tau}^{-\theta} \end{pmatrix} \quad \text{if } \alpha_{12} = \alpha_{23}, \tag{C21}$$

$$\underline{\boldsymbol{j}}_0^2 = \begin{pmatrix} \boldsymbol{\tau}_2 & 0 \\ 0 & 0 \end{pmatrix}, \tag{C22}$$

$$\underline{\boldsymbol{j}}_0^3 = \begin{pmatrix} \frac{\alpha_{23}^2}{\lambda^2}\boldsymbol{\tau}_1 & -\frac{\alpha_{12}\alpha_{23}}{\lambda^2}\boldsymbol{\tau}_c \\ -\frac{\alpha_{12}\alpha_{23}}{\lambda^2}\boldsymbol{\tau}_c^\dagger & \frac{\alpha_{12}^2}{\lambda^2}\boldsymbol{\tau}^{-\theta} \end{pmatrix}$$
$$= \frac{1}{2}\begin{pmatrix} \boldsymbol{\tau}_1 & -\boldsymbol{\tau}_c \\ -\boldsymbol{\tau}_c^\dagger & \boldsymbol{\tau}^{-\theta} \end{pmatrix} \quad \text{if } \alpha_{12} = \alpha_{23}, \tag{C23}$$

where

$$\boldsymbol{\tau}_1 = \begin{pmatrix} \boldsymbol{\tau}^{-\theta} & 0 \\ 0 & 0 \end{pmatrix}, \quad \boldsymbol{\tau}_2 = \begin{pmatrix} 0 & 0 \\ 0 & \boldsymbol{\tau}^{\theta} \end{pmatrix},$$

$$\boldsymbol{\tau}_c = \begin{pmatrix} \boldsymbol{\tau}^{-\theta} \\ 0 \end{pmatrix}.$$

In fact, the 4×2 matrix $\boldsymbol{\tau}_c$ is responsible for $\boldsymbol{\sigma}_c$.

Thus, in the interaction picture we have

$$\underline{\boldsymbol{j}}^1(t) = \frac{1}{\lambda^2}\begin{pmatrix} \alpha_{12}^2 e^{i\mathcal{H}_2t}\boldsymbol{\tau}_1 e^{-i\mathcal{H}_2t} & \alpha_{12}\alpha_{23}e^{i\mathcal{H}_2t}\boldsymbol{\tau}_c e^{-i\mathcal{H}_1t} \\ \alpha_{12}\alpha_{23}e^{i\mathcal{H}_1t}\boldsymbol{\tau}_c^\dagger e^{-i\mathcal{H}_2t} & \alpha_{23}^2 e^{i\mathcal{H}_1t}\boldsymbol{\tau}^{-\theta}e^{-i\mathcal{H}_1t} \end{pmatrix},$$

$$\underline{\boldsymbol{j}}^2(t) = \begin{pmatrix} e^{i\mathcal{H}_2t}\boldsymbol{\tau}_2 e^{-i\mathcal{H}_2t} & 0 \\ 0 & 0 \end{pmatrix},$$

$$\underline{\boldsymbol{j}}^3(t) = \frac{1}{\lambda^2}\begin{pmatrix} \alpha_{23}^2 e^{i\mathcal{H}_2t}\boldsymbol{\tau}_1 e^{-i\mathcal{H}_2t} & -\alpha_{12}\alpha_{23}e^{i\mathcal{H}_2t}\boldsymbol{\tau}_c e^{-i\mathcal{H}_1t} \\ -\alpha_{12}\alpha_{23}e^{i\mathcal{H}_1t}\boldsymbol{\tau}_c^\dagger e^{-i\mathcal{H}_2t} & \alpha_{12}^2 e^{i\mathcal{H}_1t}\boldsymbol{\tau}^{-\theta}e^{-i\mathcal{H}_1t} \end{pmatrix}.$$

By abusing notation, we define the frequencies

$$\omega_{\eta\eta'} = (E_\eta - E_{\eta'})/\hbar,$$

where $E_{\eta(\eta')}$ is the energy of either the effective single-layer or twisted bilayer system. The frequency ω_{bs} mixes these energies, and will appear in $\boldsymbol{\sigma}_c$ (Appendix C 3).

Let us now outline the steps for the remaining computation of $[\underline{\boldsymbol{j}}^{\ell}(t), \underline{\boldsymbol{j}}_0^{\ell}]$. For every pair (ℓ, ℓ') we use the matrices $V_{\eta\eta'}^{\ell\ell'}$ from Eq. (C2), needed for $\eta = \eta'$. Note that the Hermitian adjoint of this expression reads

$$\underline{\boldsymbol{j}}_0^{\ell'}\underline{\boldsymbol{j}}^{\ell}(t) = \begin{pmatrix} V_{bb}^{\ell\ell'}(t)^\dagger & V_{sb}^{\ell\ell'}(t)^\dagger \\ V_{bs}^{\ell\ell'}(t)^\dagger & V_{ss}^{\ell\ell'}(t)^\dagger \end{pmatrix}.$$

Thus, it suffices to determine $\underline{j}^{\ell}(t)\underline{j}_0^{\ell'}$. The matrix elements of $[\underline{j}^{\ell}(t), \underline{j}_0^{\ell'}]$ are found from $V_{\eta\eta'}^{\ell\ell'}(t) - (V_{\eta\eta'}^{\ell\ell'}(t))^{\dagger}$.

a. Tensor $V_{\eta\eta'}^{11}$

For $(\ell, \ell') = (1, 1)$, the diagonal block matrix of the first layer, $[\underline{j}^1(t), \underline{j}_0^1]$ directly comes from the following formulas. Regarding $\underline{j}^1(t)\underline{j}_0^1$, we compute

$$V_{bb}^{11} = \frac{\alpha_{12}^2}{\lambda^4}\left(\alpha_{12}^2 e^{i\mathcal{H}_2 t}\boldsymbol{\tau}_1 e^{-i\mathcal{H}_2 t}\boldsymbol{\tau}_1 + \alpha_{23}^2 e^{i\mathcal{H}_2 t}\boldsymbol{\tau}_c e^{-i\mathcal{H}_1 t}\boldsymbol{\tau}_c^{\dagger}\right),$$

$$V_{bs}^{11} = \frac{\alpha_{12}\alpha_{23}}{\lambda^4}\left(\alpha_{12}^2 e^{i\mathcal{H}_2 t}\boldsymbol{\tau}_1 e^{-i\mathcal{H}_2 t}\boldsymbol{\tau}_c + \alpha_{23}^2 e^{i\mathcal{H}_2 t}\boldsymbol{\tau}_c e^{-i\mathcal{H}_1 t}\boldsymbol{\tau}^{-\theta}\right),$$

$$V_{sb}^{11} = \frac{\alpha_{12}\alpha_{23}}{\lambda^4}\left(\alpha_{12}^2 e^{i\mathcal{H}_1 t}\boldsymbol{\tau}_c^{\dagger} e^{-i\mathcal{H}_2 t}\boldsymbol{\tau}_1 + \alpha_{23}^2 e^{i\mathcal{H}_1 t}\boldsymbol{\tau}^{-\theta} e^{-i\mathcal{H}_1 t}\boldsymbol{\tau}_c^{\dagger}\right),$$

$$V_{ss}^{11} = \frac{\alpha_{23}^2}{\lambda^4}\left(\alpha_{12}^2 e^{i\mathcal{H}_1 t}\boldsymbol{\tau}_c^{\dagger} e^{-i\mathcal{H}_2 t}\boldsymbol{\tau}_c + \alpha_{23}^2 e^{i\mathcal{H}_t}\boldsymbol{\tau}^{-\theta} e^{-i\mathcal{H}_1 t}\boldsymbol{\tau}^{-\theta}\right).$$

The product $\underline{j}_0^1\underline{j}^1(t)$ is thus determined by

$$\left(V_{bb}^{11}\right)^{\dagger} = \frac{\alpha_{12}^2}{\lambda^4}\left(\alpha_{12}^2\boldsymbol{\tau}_1 e^{i\mathcal{H}_2 t}\boldsymbol{\tau}_1 e^{-i\mathcal{H}_2 t} + \alpha_{23}^2\boldsymbol{\tau}_c e^{i\mathcal{H}_1 t}\boldsymbol{\tau}_c^{\dagger} e^{-i\mathcal{H}_2 t}\right),$$

$$\left(V_{sb}^{11}\right)^{\dagger} = \frac{\alpha_{12}\alpha_{23}}{\lambda^4}\left(\alpha_{12}^2\boldsymbol{\tau}_1 e^{i\mathcal{H}_2 t}\boldsymbol{\tau}_c e^{-i\mathcal{H}_1 t} + \alpha_{23}^2\boldsymbol{\tau}_c e^{i\mathcal{H}_1 t}\boldsymbol{\tau}^{-\theta} e^{-i\mathcal{H}_1 t}\right),$$

$$\left(V_{bs}^{11}\right)^{\dagger} = \frac{\alpha_{12}\alpha_{23}}{\lambda^4}\left(\alpha_{12}^2\boldsymbol{\tau}_c^{\dagger} e^{i\mathcal{H}_2 t}\boldsymbol{\tau}_1 e^{-i\mathcal{H}_2 t} + \alpha_{23}^2\boldsymbol{\tau}^{-\theta} e^{i\mathcal{H}_1 t}\boldsymbol{\tau}_c^{\dagger} e^{-i\mathcal{H}_2 t}\right),$$

$$\left(V_{ss}^{11}\right)^{\dagger} = \frac{\alpha_{23}^2}{\lambda^4}\left(\alpha_{12}^2\boldsymbol{\tau}_c^{\dagger} e^{i\mathcal{H}_2 t}\boldsymbol{\tau}_c e^{-i\mathcal{H}_1 t} + \alpha_{23}^2\boldsymbol{\tau}^{-\theta} e^{i\mathcal{H}_1 t}\boldsymbol{\tau}^{-\theta} e^{-i\mathcal{H}_1 t}\right).$$

The commutator $[\underline{j}^1(t), \underline{j}_0^1]$ is then readily computed.

b. Tensors $V_{\eta\eta'}^{12}$ and $V_{\eta\eta'}^{21}$

Let us now discuss the structure of both $[\underline{j}^1(t), \underline{j}_0^2]$ and $[\underline{j}^2(t), \underline{j}_0^1]$. For the product $\underline{j}^1(t)\underline{j}_0^2$, we compute

$$V_{bb}^{12} = \frac{\alpha_{12}^2}{\lambda^2}e^{i\mathcal{H}_2 t}\boldsymbol{\tau}_1 e^{-i\mathcal{H}_2 t}\boldsymbol{\tau}_2,$$

$$V_{sb}^{12} = \frac{\alpha_{12}\alpha_{23}}{\lambda^2}e^{i\mathcal{H}_1 t}\boldsymbol{\tau}_c^{\dagger} e^{-i\mathcal{H}_2 t}\boldsymbol{\tau}_2,$$

$$V_{bs}^{12} = 0 = V_{ss}^{12}.$$

Similarly, for $\underline{j}_0^2\underline{j}^1(t)$ we invoke the Hermitian conjugate (adjoint) of each of the above quantities.

For $[\underline{j}^2(t), \underline{j}_0^1]$, a similar calculation yields

$$V_{bb}^{21} = \frac{\alpha_{12}^2}{\lambda^2}e^{i\mathcal{H}_2 t}\boldsymbol{\tau}_2 e^{-i\mathcal{H}_2 t}\boldsymbol{\tau}_1,$$

$$V_{bs}^{21} = \frac{\alpha_{12}\alpha_{23}}{\lambda^2}e^{i\mathcal{H}_2 t}\boldsymbol{\tau}_2 e^{-i\mathcal{H}_2 t}\boldsymbol{\tau}_c,$$

$$V_{sb}^{21} = 0 = V_{ss}^{21}.$$

The Hermitian conjugate of each term follows directly.

c. Tensors $V_{\eta\eta'}^{13}$ and $V_{\eta\eta'}^{31}$

Next, we focus on $[\underline{j}^1(t), \underline{j}_0^3]$ and $[\underline{j}^3(t), \underline{j}_0^1]$. For the former, the product $\underline{j}^1(t)\underline{j}_0^3$ is composed of

$$V_{bb}^{13} = \frac{\alpha_{12}^2\alpha_{23}^2}{\lambda^4}\left(e^{i\mathcal{H}_2 t}\boldsymbol{\tau}_1 e^{-i\mathcal{H}_2 t}\boldsymbol{\tau}_1 - e^{i\mathcal{H}_2 t}\boldsymbol{\tau}_c e^{-i\mathcal{H}_1 t}\boldsymbol{\tau}_c^{\dagger}\right),$$

$$V_{bs}^{13} = \frac{\alpha_{12}^3\alpha_{23}}{\lambda^4}\left(e^{i\mathcal{H}_2 t}\boldsymbol{\tau}_c e^{-i\mathcal{H}_1 t}\boldsymbol{\tau}^{-\theta} - e^{i\mathcal{H}_2 t}\boldsymbol{\tau}_1 e^{-i\mathcal{H}_2 t}\boldsymbol{\tau}_c\right),$$

$$V_{sb}^{13} = \frac{\alpha_{12}\alpha_{23}^3}{\lambda^4}\left(e^{i\mathcal{H}_1 t}\boldsymbol{\tau}_c^{\dagger} e^{-i\mathcal{H}_2 t}\boldsymbol{\tau}_1 - e^{i\mathcal{H}_1 t}\boldsymbol{\tau}^{-\theta} e^{-i\mathcal{H}_1 t}\boldsymbol{\tau}_c^{\dagger}\right),$$

$$V_{ss}^{13} = \frac{\alpha_{12}^2\alpha_{23}^2}{\lambda^4}\left(e^{i\mathcal{H}_1 t}\boldsymbol{\tau}^{-\theta} e^{-i\mathcal{H}_1 t}\boldsymbol{\tau}^{-\theta} - e^{i\mathcal{H}_1 t}\boldsymbol{\tau}_c^{\dagger} e^{-i\mathcal{H}_2 t}\boldsymbol{\tau}_c\right).$$

For $\underline{j}_0^3\underline{j}^1(t)$, we compute the Hermitian adjoints.

On the other hand, in regard to $[\underline{j}^3(t), \underline{j}_0^1]$ we obtain

$$V_{bb}^{31} = \frac{\alpha_{12}^2\alpha_{23}^2}{\lambda^4}\left(e^{i\mathcal{H}_2 t}\boldsymbol{\tau}_1 e^{-i\mathcal{H}_2 t}\boldsymbol{\tau}_1 - e^{i\mathcal{H}_2 t}\boldsymbol{\tau}_c e^{-i\mathcal{H}_1 t}\boldsymbol{\tau}_c^{\dagger}\right),$$

$$V_{bs}^{31} = \frac{\alpha_{12}\alpha_{23}^3}{\lambda^4}\left(e^{i\mathcal{H}_2 t}\boldsymbol{\tau}_1 e^{-i\mathcal{H}_2 t}\boldsymbol{\tau}_c - e^{i\mathcal{H}_2 t}\boldsymbol{\tau}_c e^{-i\mathcal{H}_1 t}\boldsymbol{\tau}^{-\theta}\right),$$

$$V_{sb}^{31} = \frac{\alpha_{12}^3\alpha_{23}}{\lambda^4}\left(e^{i\mathcal{H}_1 t}\boldsymbol{\tau}^{-\theta} e^{-i\mathcal{H}_1 t}\boldsymbol{\tau}_c^{\dagger} - e^{i\mathcal{H}_1 t}\boldsymbol{\tau}_c^{\dagger} e^{-i\mathcal{H}_2 t}\boldsymbol{\tau}_1\right),$$

$$V_{ss}^{31} = \frac{\alpha_{12}^2\alpha_{23}^2}{\lambda^4}\left(e^{i\mathcal{H}_1 t}\boldsymbol{\tau}^{-\theta} e^{-i\mathcal{H}_1 t}\boldsymbol{\tau}^{-\theta} - e^{i\mathcal{H}_1 t}\boldsymbol{\tau}_c^{\dagger} e^{-i\mathcal{H}_2 t}\boldsymbol{\tau}_c\right),$$

along with their Hermitian conjugates. This step concludes the calculation for $(\ell, \ell') = (1, 3), (3, 1)$.

d. Tensor $V_{\eta\eta'}^{22}$

Consider the diagonal block matrix of the middle layer, related to $[\underline{j}^2(t), \underline{j}_0^2]$. For $\underline{j}^2(t)\underline{j}_0^2$, we need

$$V_{bb}^{22} = e^{i\mathcal{H}_2 t}\boldsymbol{\tau}_2 e^{-i\mathcal{H}_2 t}\boldsymbol{\tau}_2,$$

$$V_{bs}^{22} = 0 = V_{sb}^{22} = V_{ss}^{22}.$$

The Hermitian adjoint, for $\underline{j}_0^2\underline{j}^2(t)$, follows directly.

e. Tensors $V_{\eta\eta'}^{23}$ and $V_{\eta\eta'}^{32}$

For layers 2 and 3, we first compute

$$V_{bb}^{23} = \frac{\alpha_{23}^2}{\lambda^2}e^{i\mathcal{H}_2 t}\boldsymbol{\tau}_2 e^{-i\mathcal{H}_2 t}\boldsymbol{\tau}_1,$$

$$V_{bs}^{23} = -\frac{\alpha_{12}\alpha_{23}}{\lambda^2}e^{i\mathcal{H}_2 t}\boldsymbol{\tau}_2 e^{-i\mathcal{H}_2 t}\boldsymbol{\tau}_c,$$

$$V_{sb}^{23} = 0 = V_{ss}^{23}.$$

Likewise, we have

$$V_{bb}^{32} = \frac{\alpha_{23}^2}{\lambda^2}e^{i\mathcal{H}_2 t}\boldsymbol{\tau}_1 e^{-i\mathcal{H}_2 t}\boldsymbol{\tau}_2,$$

$$V_{sb}^{32} = -\frac{\alpha_{12}\alpha_{23}}{\lambda^2}e^{i\mathcal{H}_1 t}\boldsymbol{\tau}_c^{\dagger} e^{-i\mathcal{H}_2 t}\boldsymbol{\tau}_2,$$

$$V_{bs}^{32} = 0 = V_{ss}^{32}.$$

f. Tensor $V_{\eta\eta'}^{33}$

For the diagonal block matrix of the third (top) layer, a direct computation yields

$$V_{bb}^{33} = \frac{\alpha_{23}^2}{\lambda^4}\left(\alpha_{23}^2 e^{i\mathcal{H}_2 t}\boldsymbol{\tau}_1 e^{-i\mathcal{H}_2 t}\boldsymbol{\tau}_1 + \alpha_{12}^2 e^{i\mathcal{H}_2 t}\boldsymbol{\tau}_c e^{-i\mathcal{H}_1 t}\boldsymbol{\tau}_c^\dagger\right),$$

$$V_{bs}^{33} = -\frac{\alpha_{23}\alpha_{23}}{\lambda^4}\left(\alpha_{23}^2 e^{i\mathcal{H}_2 t}\boldsymbol{\tau}_1 e^{-i\mathcal{H}_2 t}\boldsymbol{\tau}_c + \alpha_{12}^2 e^{i\mathcal{H}_2 t}\boldsymbol{\tau}_c e^{-i\mathcal{H}_1 t}\boldsymbol{\tau}^{-\theta}\right),$$

$$V_{sb}^{33} = -\frac{\alpha_{23}\alpha_{23}}{\lambda^4}\left(\alpha_{23}^2 e^{i\mathcal{H}_1 t}\boldsymbol{\tau}_c^\dagger e^{-i\mathcal{H}_1 t}\boldsymbol{\tau}_1 + \alpha_{12}^2 e^{i\mathcal{H}_1 t}\boldsymbol{\tau}^{-\theta} e^{-i\mathcal{H}_1 t}\boldsymbol{\tau}_c^\dagger\right),$$

$$V_{ss}^{33} = \frac{\alpha_{12}^2}{\lambda^4}\left(\alpha_{23}^2 e^{i\mathcal{H}_1 t}\boldsymbol{\tau}_c^\dagger e^{-i\mathcal{H}_2 t}\boldsymbol{\tau}_c + \alpha_{12}^2 e^{i\mathcal{H}_1 t}\boldsymbol{\tau}^{-\theta} e^{-i\mathcal{H}_1 t}\boldsymbol{\tau}^{-\theta}\right).$$

3. Layer-resolved conductivity matrices

Next, we outline the remaining steps of deriving the conductivity formulas of Appendix C 1. Let

$$|s\rangle = (|\zeta_{s1}\rangle, |\zeta_{s2}\rangle)^T,$$
$$|b\rangle_1 = (|\varphi_{b1}\rangle, |\varphi_{b2}\rangle)^T, \quad |b\rangle_2 = (|\chi_{b1}\rangle, |\chi_{b2}\rangle)^T,$$

where $\zeta_{si}(\boldsymbol{x}) = \langle\boldsymbol{x}|\zeta_{si}\rangle$, $\varphi_{bi}(\boldsymbol{x}) = \langle\boldsymbol{x}|\varphi_{bi}\rangle$, and $\chi_{bi}(\boldsymbol{x}) = \langle\boldsymbol{x}|\chi_{bi}\rangle$ ($i = 1, 2$) are scalar Bloch wave functions. These are labeled by s or b which stand for the combined band index and quasimomentum variable of the scaled Brillouin zone. The spin degeneracy factor g_s is omitted here but can be included in the end.

a. σ^{11} tensor

By Eq. (C1), the structure of $\boldsymbol{\sigma}^{11}$ is dictated by the tensors $V_{\eta\eta'}^{11}$. For example, for $\eta = b$ we have the term

$$\frac{\alpha_{12}^2}{\lambda^4}\left(\alpha_{12}^2 e^{i\mathcal{H}_2 t}\boldsymbol{\tau}_1 e^{-i\mathcal{H}_2 t}\boldsymbol{\tau}_1 + \alpha_{23}^2 e^{i\mathcal{H}_2 t}\boldsymbol{\tau}_c e^{-i\mathcal{H}_1 t}\boldsymbol{\tau}_c^\dagger\right).$$

For $\eta = s$, the quantities α_{12} and α_{23}, $\mathcal{H}_1$ and $\mathcal{H}_2$, $\boldsymbol{\tau}_1$ and $\boldsymbol{\tau}^{-\theta}$, and $\boldsymbol{\tau}_c$ and $\boldsymbol{\tau}_c^\dagger$ must be, respectively, interchanged. By resolution of the identity, formula (C3) emerges once we identify the K-valley contributions

$$(\sigma_{\mathrm{BL},\nu\nu'}^{11})_K = -C_0 \frac{e^2}{i\hbar}\frac{1}{\omega + i\delta}\sum_{bb'}(f_b - f_{b'})\frac{\langle b|\tau_{1\nu}|b'\rangle\langle b'|\tau_{1\nu'}|b\rangle}{\omega + \omega_{bb'} + i\delta}, \tag{C24}$$

$$(\sigma_{\mathrm{SL},\nu\nu'}^{})_K = -C_0 \frac{e^2}{i\hbar}\frac{1}{\omega + i\delta}\sum_{ss'}(f_s - f_{s'})\frac{\langle s|\tau_\nu^{-\theta}|s'\rangle\langle s'|\tau_{\nu'}^{-\theta}|s\rangle}{\omega + \omega_{ss'} + i\delta}, \tag{C25}$$

as $\delta \downarrow 0$ for real ω. Here, we set $\tau_{(1)\nu}^{-\theta} = \mathbf{e}_\nu \cdot \boldsymbol{\tau}_{(1)}^{-\theta}$. These formulas lead to the forms $\boldsymbol{\sigma}_{\mathrm{SL}} = \mathrm{diag}(\sigma_e^{(1)}, \sigma_e^{(1)})$ and $\boldsymbol{\sigma}_{\mathrm{BL}}^{11} = \mathrm{diag}(\sigma_e^{(2)}, \sigma_e^{(2)})$, with the suitable definitions of the scalars $\sigma_e^{(1,2)}$. The coupling term $\boldsymbol{\sigma}_c$ comes from the $\boldsymbol{\tau}_c^{(\dagger)}$-matrix terms in $V_{\eta\eta}^{11}$, viz. (with $\tau_{c\nu} = \mathbf{e}_\nu \cdot \boldsymbol{\tau}_c$),

$$(\sigma_{c,\nu\nu'})_K = -C_0 \frac{e^2}{i\hbar}\frac{1}{\omega + i\delta}\sum_{bs}(f_b - f_s)$$

$$\times \left\{\frac{\langle b|\tau_{c\nu}|s\rangle\langle s|\tau_{c\nu'}^\dagger|b\rangle}{\omega + \omega_{bs} + i\delta} - \frac{\langle b|\tau_{c\nu'}|s\rangle\langle s|\tau_{c\nu}^\dagger|b\rangle}{\omega - \omega_{bs} + i\delta}\right\}.$$

We proceed to symmetrize the above quantities. For the effective single-layer system, by isotropy we have the diagonal element $\sigma_{\mathrm{SL},xx} = \sigma_{\mathrm{SL},yy} = \sigma_e^{(1)}$ with

$$\sigma_e^{(1)}(\omega) = -i2C_0 g_v \frac{e^2}{\hbar(\omega + i\delta)}\sum_{ss'}(f_s - f_{s'})\frac{\omega_{ss'}}{(\omega + i\delta)^2 - \omega_{ss'}^2}$$

$$\times |\langle\zeta_{s1}|\zeta_{s'2}\rangle|^2.$$

Here, g_v is the valley degeneracy factor ($g_v = 2$) and $\langle\zeta_{s1}|\zeta_{s'2}\rangle$ stands for the inner product of the scalar Bloch wave functions $\zeta_{1,2}^{s,s'}(\boldsymbol{x})$ over the scaled cell. For the off-diagonal elements $\sigma_{\mathrm{SL},xy}$ and $\sigma_{\mathrm{SL},yx}$, symmetrization and the effect of isotropy yield

$$\sigma_{\mathrm{SL},xy}(\omega) = -\sigma_{\mathrm{SL},yx}(\omega) = 0.$$

Similarly, for the effective twisted bilayer system, by isotropy we have $\sigma_{\mathrm{BL},xx}^{11} = \sigma_{\mathrm{BL},yy}^{11} = \sigma_e^{(2)}$ where

$$\sigma_e^{(2)}(\omega) = -i2C_0 g_v \frac{e^2}{\hbar(\omega + i\delta)}\sum_{bb'}(f_b - f_{b'})$$

$$\times \frac{\omega_{bb'}}{(\omega + i\delta)^2 - \omega_{bb'}^2}|\langle\varphi_{b1}|\varphi_{b'2}\rangle|^2.$$

The calculation for $\sigma_{\mathrm{BL},xy}^{11}$ and $\sigma_{\mathrm{BL},yx}^{11}$ makes explicit use of time-reversal symmetry and isotropy, yielding

$$\sigma_{\mathrm{BL},xy}^{11}(\omega) = -\sigma_{\mathrm{BL},yx}^{11}(\omega) = 0.$$

Let us consider $\boldsymbol{\sigma}_c$. For its diagonal elements, we get

$$\left(\sigma_{c,\,yy}^{\,xx}\right)_K = -2iC_0 \frac{e^2}{\hbar(\omega + i\delta)}\sum_{bs}(f_b - f_s)$$

$$\times \frac{\omega_{bs}}{(\omega + i\delta)^2 - \omega_{bs}^2}|\langle\check{\varphi}_{b1}|\zeta_{s2}\rangle \pm \langle\varphi_{b2}|\check{\zeta}_{s1}\rangle|^2,$$

where $\check{\varpi} = e^{i\theta/2}\varpi$ for $\varpi = \varphi_{b1}, \zeta_{s1}$. By isotropy, we have $\sigma_{c,xx}(\omega) - \sigma_{c,yy}(\omega) = 0$ which implies

$$\sum_{bs}(f_b - f_s)\frac{\omega_{bs}}{(\omega + i\delta)^2 - \omega_{bs}^2}\mathrm{Re}(\langle\check{\varphi}_{b1}|\zeta_{s2}\rangle\langle\check{\zeta}_{s1}|\varphi_{b2}\rangle) = 0; \tag{C26}$$

thus, $\sigma_{c,xx} = \sigma_{c,yy} = \sigma_c$ where

$$\sigma_c(\omega) = -i2C_0 g_v \frac{e^2}{\hbar(\omega + i\delta)}\sum_{bs}(f_b - f_s)\frac{\omega_{bs}}{(\omega + i\delta)^2 - \omega_{bs}^2}$$

$$\times (|\langle\varphi_{b1}|\zeta_{s2}\rangle|^2 + |\langle\varphi_{b2}|\zeta_{s1}\rangle|^2). \tag{C27}$$

This expression can be simplified by use of $|\langle\varphi_{b1}|\zeta_{s2}\rangle| = |\langle\zeta_{s1}|\varphi_{b2}\rangle|$ due to the invariance of $\mathcal{H}_{1,2}$ under the combined operations of sublattice index switch, complex conjugation, and parity inversion.

For the off-diagonal elements of $\boldsymbol{\sigma}_c$, we assert that

$$\left(\sigma_{c,\,yx}^{\,xy}\right)_K = 2C_0 \frac{e^2}{\hbar(\omega + i\delta)}\sum_{bs}(f_b - f_s)$$

$$\times \frac{\mp(\omega + i\delta)\mathrm{Re}(m_{bs}^{\varphi\zeta}) + i\omega_{bs}\mathrm{Im}(m_{bs}^{\varphi\zeta})}{(\omega + i\delta)^2 - \omega_{bs}^2}, \quad \delta \downarrow 0;$$

$$m_{bs}^{\varphi\zeta} = (\langle\check{\varphi}_{b1}|\zeta_{s2}\rangle + \langle\varphi_{b2}|\check{\zeta}_{s1}\rangle)(\langle\zeta_{s2}|\check{\varphi}_{b1}\rangle - \langle\check{\zeta}_{s1}|\varphi_{b2}\rangle).$$

By symmetrizing this K-valley contribution, we obtain

$$\sigma_{c,xy}(\omega) = \sigma_{c,yx}(\omega) = i2C_0 g_v \frac{e^2}{\hbar(\omega + i\delta)}$$

$$\times \sum_{bs}(f_b - f_s)\frac{\omega_{bs}}{(\omega + i\delta)^2 - \omega_{bs}^2}\,\text{Im}\big(m_{bs}^{\varphi\zeta}\big).$$

Notice that $\text{Im}(m_{bs}^{\varphi\zeta}) = -2\,\text{Im}(\langle\check\varphi_{b1}|\zeta_{s2}\rangle\langle\check\zeta_{s1}|\varphi_{b2}\rangle)$. In view of identity (C26), along with the interchange of the Re($\cdot$) and Im($\cdot$) factors in it, we infer that $\sigma_{c,xy}(\omega) = 0 = \sigma_{c,yx}(\omega)$. Alternatively, this vanishing of the off-diagonal elements of $\boldsymbol\sigma_c$ results from isotropy, by which $\sigma_{c,xy}(\omega) = -\sigma_{c,yx}(\omega)$. Equations (C4) and (C11) follow.

b. σ^{12} and σ^{21} tensors

Next, we address the cases of layer pairs $(\ell, \ell') = (1, 2)$, $(2, 1)$. Because each of $V_{bb}^{12,21}$ contains only one product with $\boldsymbol\tau_{1,2}$ and is multiplied by $\alpha_{12}^2\lambda^{-2}$, while $V_{ss}^{12,21} = 0$, we see that each of $\boldsymbol\sigma^{12,21}$ is proportional to $\boldsymbol\sigma_{\text{BL}}^{12,21}$. For the K-valley term, Eq. (C1) implies

$$\boldsymbol\sigma_K^{12(21)} = \frac{\alpha_{12}^2}{\lambda^2}\big(\boldsymbol\sigma_{\text{BL}}^{12(21)}\big)_K,$$

where

$$\big(\sigma_{\text{BL},\nu\nu'}^{12(21)}\big)_K = -C_0\frac{e^2}{\hbar(\omega + i\delta)}\sum_{bb'}(f_b - f_{b'})$$

$$\times \frac{\langle b|\tau_{1(2)\nu}|b'\rangle\langle b'|\tau_{2(1)\nu'}|b\rangle}{i(\omega + i\delta + \omega_{bb'})}.$$

For the diagonal elements, symmetrization entails

$$\sigma_{\text{BL},\,xx\atop yy}^{12} = \sigma_{\text{BL},\,xx\atop yy}^{21} = -i2C_0 g_v\frac{e^2}{\hbar(\omega + i\delta)}\sum_{bb'}(f_b - f_{b'})$$

$$\times \frac{\omega_{bb'}\,\text{Re}\{(\langle\check\varphi_{b1}|\varphi_{b'2}\rangle \pm \langle\varphi_{b2}|\check\varphi_{b'1}\rangle)\langle\check\chi_{b'2}|\chi_{b1}\rangle\}}{(\omega + i\delta)^2 - \omega_{bb'}^2}.$$

By isotropy, which means $\sigma_{\text{BL},xx}^{12(21)} - \sigma_{\text{BL},yy}^{12(21)} = 0$, we have

$$\sum_{bb'}(f_b - f_{b'})\frac{\omega_{bb'}\,\text{Re}(\langle\check\varphi_{b1}|\varphi_{b'2}\rangle\langle\chi_{b'2}|\check\chi_{b2}\rangle)}{(\omega + i\delta)^2 - \omega_{bb'}^2} = 0; \quad \text{(C28)}$$

therefore, we can set $\sigma_{\text{BL},xx}^{12(21)} = \sigma_{\text{BL},yy}^{12(21)} = \sigma_e^{12}$ where

$$\sigma_e^{12}(\omega) = -i2C_0 g_v\frac{e^2}{\hbar(\omega + i\delta)}\sum_{bb'}(f_b - f_{b'})$$

$$\times \frac{\omega_{bb'}\,\text{Re}(e^{-i\theta}\langle\varphi_{b1}|\varphi_{b'2}\rangle\langle\chi_{b'2}|\chi_{b1}\rangle)}{(\omega + i\delta)^2 - \omega_{bb'}^2}. \quad \text{(C29)}$$

Regarding the off-diagonal elements of $\boldsymbol\sigma^{12}$, we find

$$\sigma_{\text{BL},\,xy\atop yx}^{12} = \sigma_{\text{BL},\,yx\atop xy}^{21} = \pm i2C_0 g_v\frac{e^2}{\hbar(\omega + i\delta)}\sum_{bb'}(f_b - f_{b'})$$

$$\times \frac{\omega_{bb'}\,\text{Im}\{(\langle\check\chi_{b'2}|\chi_{b1}\rangle \mp \langle\chi_{b'1}|\check\chi_{b2}\rangle)\langle\check\varphi_{b1}|\varphi_{b'2}\rangle\}}{(\omega + i\delta)^2 - \omega_{bb'}^2}.$$

Note that $\sigma_{\text{BL},\,xy\atop yx}^{12(21)} + \sigma_{\text{BL},\,yx\atop xy}^{12(21)} = 0$, inferred from Eq. (C28) by replacement of Re($\cdot$) by Im($\cdot$); thus, $\sigma_{\text{BL},\,xy\atop yx}^{12(21)} = -\sigma_{\text{BL},\,yx\atop xy}^{12(21)} = \sigma_{e,xy}^{12}$

with

$$\sigma_{e,xy}^{12}(\omega) = i2C_0 g_v\frac{e^2}{\hbar(\omega + i\delta)}\sum_{bb'}(f_b - f_{b'})$$

$$\times \frac{\omega_{bb'}\,\text{Im}(e^{-i\theta}\langle\chi_{b'2}|\chi_{b1}\rangle\langle\varphi_{b1}|\varphi_{b'2}\rangle)}{(\omega + i\delta)^2 - \omega_{bb'}^2}. \quad \text{(C30)}$$

Equations (C5) and (C12) follow.

c. σ^{13} and σ^{31} tensors

Consider $(\ell, \ell') = (1, 3)$ and $(3,1)$. By Eq. (C1), $\boldsymbol\sigma^{13,31}$ contain contributions from the two effective systems and the coupling term $\boldsymbol\sigma_c$ that are similar to those for $\boldsymbol\sigma^{11}$. By inspection of $V_{\eta\eta}^{13,31}$ in comparison to $V_{\eta\eta}^{11}$, from Eq. (C1) we can derive Eq. (C6).

In more detail, for $\alpha_{12} = \alpha_{23}$, we see that

$$V_{bb}^{11} = \tfrac{1}{4}\big(e^{i\mathcal H_2 t}\boldsymbol\tau_1 e^{-i\mathcal H_2 t}\boldsymbol\tau_1 + e^{i\mathcal H_2 t}\boldsymbol\tau_c e^{-i\mathcal H_1 t}\boldsymbol\tau_c^\dagger\big),$$

whereas

$$V_{bb}^{13} = \tfrac{1}{4}\big(e^{i\mathcal H_2 t}\boldsymbol\tau_1 e^{-i\mathcal H_2 t}\boldsymbol\tau_1 - e^{i\mathcal H_2 t}\boldsymbol\tau_c e^{-i\mathcal H_1 t}\boldsymbol\tau_c^\dagger\big) = V_{bb}^{31};$$

ditto for $V_{ss}^{11,13}$ via the switch of $\mathcal H_2$ and $\mathcal H_1$, $\boldsymbol\tau_1$ and $\boldsymbol\tau^{-\theta}$, and $\boldsymbol\tau_c$ and its Hermitian adjoint. Thus, in the case with mirror symmetry, the matrix $\boldsymbol\sigma^{11}$ of Eq. (C16) is replaced by the $\boldsymbol\sigma^{13}$ given in Eq. (C18).

Now consider $\alpha_{12} \neq \alpha_{23}$. Notice the terms in

$$V_{bb(ss)}^{11} = \frac{\alpha_{12(23)}^2}{\lambda^4}\big(\alpha_{12(23)}^2 e^{i\mathcal H_{2(1)}t}\boldsymbol\tau_1^{(-\theta)}e^{-i\mathcal H_{2(1)}t}\boldsymbol\tau_1^{(-\theta)}$$

$$+ \alpha_{23(12)}^2 e^{i\mathcal H_{2(1)}t}\boldsymbol\tau_c^{(\dagger)}e^{-i\mathcal H_{1(2)}t}\boldsymbol\tau_c^{\dagger()}\big),$$

and map this to its 13- (and 31-) counterpart, viz.,

$$V_{bb(ss)}^{13} = \frac{\alpha_{12}^2\alpha_{23}^2}{\lambda^4}\big(e^{i\mathcal H_{2(1)}t}\boldsymbol\tau_1^{(-\theta)}e^{-i\mathcal H_{2(1)}t}\boldsymbol\tau_1^{(-\theta)}$$

$$- e^{i\mathcal H_2 t}\boldsymbol\tau_c^{(\dagger)}e^{-i\mathcal H_{1(2)}t}\boldsymbol\tau_c^{\dagger()}\big).$$

Equation (C6) results from Eq. (C3) via this map.

d. σ^{22} tensor

By inspection of $V_{\eta\eta}^{22}$, we notice that $\boldsymbol\sigma^{22}$ is identical to $\boldsymbol\sigma_{\text{BL}}^{22}$ according to the expression

$$\big(\sigma_{\text{BL},\nu\nu'}^{22}\big)_K = -C_0\frac{e^2}{\hbar(\omega + i\delta)}\sum_{bb'}(f_b - f_{b'})\frac{\langle b|\tau_{2\nu}|b'\rangle\langle b'|\tau_{2\nu'}|b\rangle}{i(\omega + \omega_{bb'} + i\delta)},$$
$$\text{(C31)}$$

which comes from Eq. (C24) after the replacement of $\boldsymbol\tau_1$ by $\boldsymbol\tau_2$. The resulting expression for $\boldsymbol\sigma^{22} = \boldsymbol\sigma_{\text{BL}}^{22}$ depends on $\alpha_{12,23}$ through the effective Hamiltonian $\mathcal H_2$, and is a diagonal matrix (as is $\boldsymbol\sigma_{\text{BL}}^{11}$). Thus, we obtain Eq. (C8). The nonzero (diagonal) elements of $\boldsymbol\sigma_{\text{BL}}^{22}$ come from $\sigma_e^{(2)}$ by replacement of $\varphi_{1,2}$ by $\chi_{1,2}$:

$$\sigma_{\text{BL},xx}^{22} = \sigma_{\text{BL},yy}^{22} = -i2C_0 g_v\frac{e^2}{\hbar(\omega + i\delta)}\sum_{bb'}(f_b - f_{b'})$$

$$\times \frac{\omega_{bb'}}{(\omega + i\delta)^2 - \omega_{bb'}^2}|\langle\chi_{b1}|\chi_{b'2}\rangle|^2$$

$$= \sigma_0^{22} = \sigma_e^{(2)}.$$

In the above, we assumed that $|\langle\chi_{b1}|\chi_{b'2}\rangle| = |\langle\varphi_{b1}|\varphi_{b'2}\rangle|$ since $\mathcal{H}_{2,K}$ is invariant under the simultaneous operations of layer switch, complex conjugation, and x-direction reversal.

e. σ^{23}, σ^{32}, and σ^{33} tensors

Let us first consider σ^{23} and σ^{32}. Evidently, $V_{\eta\eta}^{23,32}$ come from $V_{\eta\eta}^{21,12}$ under the replacement of α_{12} with α_{23}. By a rescaling and transposition of formula (C5), we obtain Eq. (C9). Recall that time-reversal symmetry dictates $\sigma_{\mathrm{BL}}^{12}(\omega) = \sigma_{\mathrm{BL}}^{21}(\omega)^T$.

Regarding σ^{33}, notice that $V_{\eta\eta}^{33}$ results from $V_{\eta\eta}^{11}$ by switch of the parameters α_{12} and α_{23}. This implies that Eq. (C3) yields Eq. (C10). Hence, matrix σ^{33} is diagonal. We set $\sigma^{33} = \mathrm{diag}(\sigma_0^{33}, \sigma_0^{33})$ where the scalar $\sigma_0^{33}(\omega)$ directly comes from $\sigma_0^{11}(\omega)$ by the interchange of α_{12} and α_{23} [cf. Eqs. (C11) and (C15)].

APPENDIX D: IN-PLANE CURRENTS AS MAGNETIZATION CURRENTS

In this Appendix, we show that the in-plane currents of any number (n) of layers can always be written as the sum of the average current plus *magnetization* currents. The latter are imagined as coming from filling the space between adjacent layers with uniformly, in-plane magnetized materials. The electric currents ($\mathbf{J}_i$) are numbered from bottom to top,

as in Fig. 1 for $n = 3$. As in Sec. III B, we use the symbol $\mathbf{m}_i$ to describe the magnetic moment (per unit surface) of the (imagined) magnetized material filling the space between layers i and $i+1$. For the reference case of the trilayer system ($n = 3$), we have three currents $\{\mathbf{J}_1, \mathbf{J}_2, \mathbf{J}_3\}$ and two magnetized regions with magnetic moments per unit surface $\{\mathbf{m}_1, \mathbf{m}_2\}$, filling the space between layers 1 and 2, and layers 2 and 3, respectively.

We can always write

$$\mathbf{J}_i = \frac{\mathbf{J}_{\mathrm{tot}}}{n} + \mathbf{j}_i, \tag{D1}$$

where $\mathbf{J}_{\mathrm{tot}} = \sum_i \mathbf{J}_i$ is the total current, and $\mathbf{j}_i$ represents the deviation from the average. Given that $\sum_i \mathbf{j}_i = 0$, each $\mathbf{j}_i$ can be considered to be the sum of the magnetization currents associated with the regions above and below the layer i. Therefore, we have

$$\frac{\mathbf{m}_{i-1} - \mathbf{m}_i}{l} = \mathbf{e}_z \times \mathbf{j}_i, \quad 1 \leqslant i \leqslant n \tag{D2}$$

with the constraint $\sum_i \mathbf{j}_i = 0$, and l is the distance between layers and $\mathbf{e}_z$ the normal unit vector. In Eq. (D2), it is understood that $\mathbf{m}_i = 0$ for i outside its allowed range, that is, for $i \notin \{1, \ldots, n-1\}$. Equation (D2) provides the set of magnetizations $\{\mathbf{m}_i\}$ associated with any set of deviation currents $\{\mathbf{j}_i\}$, and vice versa. In the trilayer system, for instance, the use of Eqs. (D1) and (D2), together with $-i\omega\mathbf{p} = \mathbf{J}_{\mathrm{tot}}$, leads to Eqs. (25)–(27) of Sec. III B.

[1] Y. Cao, V. Fatemi, A. Demir, S. Fang, S. L. Tomarken, J. Y. Luo, J. D. Sanchez-Yamagishi, K. Watanabe, T. Taniguchi, E. Kaxiras, R. C. Ashoori, and P. Jarillo-Herrero, Correlated insulator behaviour at half-filling in magic-angle graphene superlattices, Nature (London) **556**, 80 (2018)..

[2] Y. Cao, V. Fatemi, S. Fang, K. Watanabe, T. Taniguchi, E. Kaxiras, and P. Jarillo-Herrero, Unconventional superconductivity in magic-angle graphene superlattices, Nature (London) **556**, 43 (2018).

[3] A. L. Sharpe, E. J. Fox, A. W. Barnard, J. Finney, K. Watanabe, T. Taniguchi, M. A. Kastner, and D. Goldhaber-Gordon, Emergent ferromagnetism near three-quarters filling in twisted bilayer graphene, Science **365**, 605 (2019).

[4] A. L. Sharpe, E. J. Fox, A. W. Barnard, J. Finney, K. Watanabe, T. Taniguchi, M. A. Kastner, and D. Goldhaber-Gordon, Evidence of orbital ferromagnetism in twisted bilayer graphene aligned to hexagonal boron nitride, Nano Lett. **21**, 4299 (2021).

[5] P. J. Ledwith, G. Tarnopolsky, E. Khalaf, and A. Vishwanath, Fractional Chern insulator states in twisted bilayer graphene: An analytical approach, Phys. Rev. Res. **2**, 023237 (2020).

[6] Y. Xie, A. T. Pierce, J. M. Park, D. E. Parker, E. Khalaf, P. Ledwith, Y. Cao, S. H. Lee, S. Chen, P. R. Forrester, K. Watanabe, T. Taniguchi, A. Vishwanath, P. Jarillo-Herrero, and A. Yacoby, Fractional Chern insulators in magic-angle twisted bilayer graphene, Nature (London) **600**, 439 (2021).

[7] A. T. Pierce, Y. Xie, J. M. Park, E. Khalaf, S. H. Lee, Y. Cao, D. E. Parker, P. R. Forrester, S. Chen, K. Watanabe, T. Taniguchi, A. Vishwanath, P. Jarillo-Herrero, and A. Yacoby,

Unconventional sequence of correlated Chern insulators in magic-angle twisted bilayer graphene, Nat. Phys. **17**, 1210 (2021).

[8] E. Suárez Morell, J. D. Correa, P. Vargas, M. Pacheco, and Z. Barticevic, Flat bands in slightly twisted bilayer graphene: Tight-binding calculations, Phys. Rev. B **82**, 121407(R) (2010).

[9] R. Bistritzer and A. H. MacDonald, Moiré bands in twisted double-layer graphene, Proc. Natl. Acad. Sci. USA **108**, 12233 (2011).

[10] E. Y. Andrei and A. H. MacDonald, Graphene bilayers with a twist, Nat. Mater. **19**, 1265 (2020).

[11] C. Jin, E. C. Regan, D. Wang, M. Iqbal Bakti Utama, C.-S. Yang, J. Cain, Y. Qin, Y. Shen, Z. Zheng, K. Watanabe, T. Taniguchi, S. Tongay, A. Zettl, and F. Wang, Identification of spin, valley and moiré quasi-angular momentum of interlayer excitons, Nat. Phys. **15**, 1140 (2019).

[12] Y. Shimazaki, I. Schwartz, K. Watanabe, T. Taniguchi, M. Kroner, and A. Imamoğlu, Strongly correlated electrons and hybrid excitons in a moiré heterostructure, Nature (London) **580**, 472 (2020).

[13] L. Wang, E.-M. Shih, A. Ghiotto, L. Xian, D. A. Rhodes, C. Tan, M. Claassen, D. M. Kennes, Y. Bai, B. Kim, K. Watanabe, T. Taniguchi, X. Zhu, J. Hone, A. Rubio, A. N. Pasupathy, and C. R. Dean, Correlated electronic phases in twisted bilayer transition metal dichalcogenides, Nat. Mater. **19**, 861 (2020).

[14] X. Wang, C. Xiao, H. Park, J. Zhu, C. Wang, T. Taniguchi, K. Watanabe, J. Yan, D. Xiao, D. R. Gamelin, W. Yao, and X. Xu, Light-induced ferromagnetism in moiré superlattices, Nature (London) **604**, 468 (2022).

[15] H. Park, J. Cai, E. Anderson, Y. Zhang, J. Zhu, X. Liu, C. Wang, W. Holtzmann, C. Hu, Z. Liu, T. Taniguchi, K. Watanabe, J.-H. Chu, T. Cao, L. Fu, W. Yao, C.-Z. Chang, D. Cobden, D. Xiao, and X. Xu, Observation of fractionally quantized anomalous Hall effect, Nature (London) **622**, 74 (2023).

[16] H. Park, J. Zhu, X. Wang, Y. Wang, W. Holtzmann, T. Taniguchi, K. Watanabe, J. Yan, L. Fu, T. Cao, D. Xiao, D. R. Gamelin, H. Yu, W. Yao, and X. Xu, Dipole ladders with large Hubbard interaction in a moiré exciton lattice, Nat. Phys. **19**, 1286 (2023).

[17] Y.-M. Wu, Z. Wu, and H. Yao, Pair-density-wave and chiral superconductivity in twisted bilayer transition metal dichalcogenides, Phys. Rev. Lett. **130**, 126001 (2023).

[18] J. Yu, J. Herzog-Arbeitman, M. Wang, O. Vafek, B. A. Bernevig, and N. Regnault, Fractional Chern insulators versus nonmagnetic states in twisted bilayer $MoTe_2$, Phys. Rev. B **109**, 045147 (2024).

[19] J. M. Park, Y. Cao, L.-Q. Xia, S. Sun, K. Watanabe, T. Taniguchi, and P. Jarillo-Herrero, Robust superconductivity in magic-angle multilayer graphene family, Nat. Mater. **21**, 877 (2022).

[20] P. J. Ledwith, A. Vishwanath, and E. Khalaf, Family of ideal Chern flatbands with arbitrary Chern number in chiral twisted graphene multilayers, Phys. Rev. Lett. **128**, 176404 (2022).

[21] A. J. Mannix, A. Ye, S. H. Sung, A. Ray, F. Mujid, C. Park, M. Lee, J.-H. Kang, R. Shreiner, A. A. High, D. A. Muller, R. Hovden, and J. Park, Robotic four-dimensional pixel assembly of van der Waals solids, Nat. Nanotechnol. **17**, 361 (2022).

[22] Z. Ji, Y. Zhao, Y. Chen, Z. Zhu, Y. Wang, W. Liu, G. Modi, E. J. Mele, S. Jin, and R. Agarwal, Opto-twistronic Hall effect in a three-dimensional spiral lattice, Nature (London) **634**, 69 (2024).

[23] J. M. Park, Y. Cao, K. Watanabe, T. Taniguchi, and P. Jarillo-Herrero, Tunable strongly coupled superconductivity in magic-angle twisted trilayer graphene, Nature (London) **590**, 249 (2021).

[24] Z. Hao, A. M. Zimmerman, P. Ledwith, E. Khalaf, D. H. Najafabadi, K. Watanabe, T. Taniguchi, A. Vishwanath, and P. Kim, Electric field-tunable superconductivity in alternating-twist magic-angle trilayer graphene, Science **371**, 1133 (2021).

[25] Y. Cao, J. M. Park, K. Watanabe, T. Taniguchi, and P. Jarillo-Herrero, Pauli-limit violation and re-entrant superconductivity in moiré graphene, Nature (London) **595**, 526 (2021).

[26] S. Carr, C. Li, Z. Zhu, E. Kaxiras, S. Sachdev, and A. Kruchkov, Ultraheavy and ultrarelativistic Dirac quasiparticles in sandwiched graphenes, Nano Lett. **20**, 3030 (2020).

[27] Z. Zhu, S. Carr, D. Massatt, M. Luskin, and E. Kaxiras, Twisted trilayer graphene: A precisely tunable platform for correlated electrons, Phys. Rev. Lett. **125**, 116404 (2020).

[28] A. Ramires and J. L. Lado, Emulating heavy fermions in twisted trilayer graphene, Phys. Rev. Lett. **127**, 026401 (2021).

[29] V. T. Phong, P. A. Pantaleón, T. Cea, and F. Guinea, Band structure and superconductivity in twisted trilayer graphene, Phys. Rev. B **104**, L121116 (2021).

[30] X. Zhang, K.-T. Tsai, Z. Zhu, W. Ren, Y. Luo, S. Carr, M. Luskin, E. Kaxiras, and K. Wang, Correlated insulating states and transport signature of superconductivity in twisted

trilayer graphene superlattices, Phys. Rev. Lett. **127**, 166802 (2021).

[31] F. Xie, N. Regnault, D. Călugăru, B. A. Bernevig, and B. Lian, Twisted symmetric trilayer graphene. II. Projected Hartree-Fock study, Phys. Rev. B **104**, 115167 (2021).

[32] A. Fischer, Z. A. H. Goodwin, A. A. Mostofi, J. Lischner, D. M. Kennes, and L. Klebl, Unconventional superconductivity in magic-angle twisted trilayer graphene, npj Quantum Mater. **7**, 5 (2022).

[33] M. Christos, S. Sachdev, and M. S. Scheurer, Correlated insulators, semimetals, and superconductivity in twisted trilayer graphene, Phys. Rev. X **12**, 021018 (2022).

[34] S. Turkel, J. Swann, Z. Zhu, M. Christos, K. Watanabe, T. Taniguchi, S. Sachdev, M. S. Scheurer, E. Kaxiras, C. R. Dean, and A. N. Pasupathy, Orderly disorder in magic-angle twisted trilayer graphene, Science **376**, 193 (2022).

[35] X. Liu, N. J. Zhang, K. Watanabe, T. Taniguchi, and J. I. A. Li, Isospin order in superconducting magic-angle twisted trilayer graphene, Nat. Phys. **18**, 522 (2022).

[36] J.-X. Lin, P. Siriviboon, H. D. Scammell, S. Liu, D. Rhodes, K. Watanabe, T. Taniguchi, J. Hone, M. S. Scheurer, and J. I. A. Li, Zero-field superconducting diode effect in small-twist-angle trilayer graphene, Nat. Phys. **18**, 1221 (2022).

[37] M. Christos, S. Sachdev, and M. S. Scheurer, Nodal band-off-diagonal superconductivity in twisted graphene superlattices, Nat. Commun. **14**, 7134 (2023).

[38] J. González and T. Stauber, Ising superconductivity induced from spin-selective valley symmetry breaking in twisted trilayer graphene, Nat. Commun. **14**, 2746 (2023).

[39] T. Devakul, P. J. Ledwith, L.-Q. Xia, A. Uri, S. C. de la Barrera, P. Jarillo-Herrero, and L. Fu, Magic-angle helical trilayer graphene, Sci. Adv. **9**, eadi6063 (2023).

[40] H. Kim, Y. Choi, É. Lantagne-Hurtubise, C. Lewandowski, A. Thomson, L. Kong, H. Zhou, E. Baum, Y. Zhang, L. Holleis, K. Watanabe, T. Taniguchi, A. F. Young, J. Alicea, and S. Nadj-Perge, Imaging inter-valley coherent order in magic-angle twisted trilayer graphene, Nature (London) **623**, 942 (2023).

[41] W. Ren, K. Davydov, Z. Zhu, J. Ma, K. Watanabe, T. Taniguchi, E. Kaxiras, M. Luskin, and K. Wang, Tunable inter-moiré physics in consecutively twisted trilayer graphene, Phys. Rev. B **110**, 115404 (2024).

[42] S. Becker, M. Embree, J. Wittsten, and M. Zworski, Mathematics of magic angles in a model of twisted bilayer graphene, Prob. Math. Phys. **3**, 69 (2022).

[43] A. B. Watson and M. Luskin, Existence of the first magic angle for the chiral model of bilayer graphene, J. Math. Phys. **62**, 091502 (2021).

[44] N. Nakatsuji, T. Kawakami, and M. Koshino, Multiscale lattice relaxation in general twisted trilayer graphenes, Phys. Rev. X **13**, 041007 (2023).

[45] F. K. Popov and G. Tarnopolsky, Magic angle butterfly in twisted trilayer graphene, Phys. Rev. Res. **5**, 043079 (2023).

[46] A. Uri, S. C. de la Barrera, M. T. Randeria, D. Rodan-Legrain, T. Devakul, P. J. D. Crowley, N. Paul, K. Watanabe, T. Taniguchi, R. Lifshitz, L. Fu, R. C. Ashoori, and P. Jarillo-Herrero, Superconductivity and strong interactions in a tunable moiré quasicrystal, Nature (London) **620**, 762 (2023).

[47] L.-Q. Xia, S. C. de la Barrera, A. Uri, A. Sharpe, Y. H. Kwan, Z. Zhu, K. Watanabe, T. Taniguchi, D. Goldhaber-Gordon, L. Fu,

T. Devakul, and P. Jarillo-Herrero, Helical trilayer graphene: A moiré platform for strongly-interacting topological bands, arXiv:2310.12204.

[48] C.-J. Kim, A. Sánchez-Castillo, Z. Ziegler, Y. Ogawa, C. Noguez, and J. Park, Chiral atomically thin films, Nat. Nanotechnol. **11**, 520 (2016).

[49] C. Ma, S. Yuan, P. Cheung, K. Watanabe, T. Taniguchi, F. Zhang, and F. Xia, Intelligent infrared sensing enabled by tunable moiré quantum geometry, Nature (London) **604**, 266 (2022).

[50] Y. Yu, K. Zhang, H. Parks, M. Babar, S. Carr, I. M. Craig, M. Van Winkle, A. Lyssenko, T. Taniguchi, K. Watanabe, V. Viswanathan, and D. K. Bediako, Tunable angle-dependent electrochemistry at twisted bilayer graphene with moiré flat bands, Nat. Chem. **14**, 267 (2022).

[51] Á. Moreno, L. Cavicchi, X. Wang, M. Peralta, M. Vergniory, K. Watanabe, T. Taniguchi, P. Jarillo-Herrero, C. Felser, M. Polini, and F. Koppens, Twisted bilayer graphene for enantiomeric sensing of chiral molecules, arXiv:2409.05178.

[52] A. Ceferino and F. Guinea, Pseudomagnetic fields in fully relaxed twisted bilayer and trilayer graphene, 2D Mater. **11**, 035015 (2024).

[53] E. Khalaf, A. J. Kruchkov, G. Tarnopolsky, and A. Vishwanath, Magic angle hierarchy in twisted graphene multilayers, Phys. Rev. B **100**, 085109 (2019).

[54] T. Stauber, T. Low, and G. Gómez-Santos, Chiral response of twisted bilayer graphene, Phys. Rev. Lett. **120**, 046801 (2018).

[55] T. Stauber, T. Low, and G. Gómez-Santos, Linear response of twisted bilayer graphene: Continuum versus tight-binding models, Phys. Rev. B **98**, 195414 (2018).

[56] T. Stauber, M. Wackerl, P. Wenk, D. Margetis, J. González, G. Gómez-Santos, and J. Schliemann, Neutral magic-angle bilayer graphene: Condon instability and chiral resonances, Small Sci. **3**, 2200080 (2023).

[57] L. Barron and J. Vrbancich, Magneto-chiral birefringence and dichroism, Mol. Phys. **51**, 715 (1984).

[58] L. D. Barron, *Molecular Light Scattering and Optical Activity* (Cambridge University Press, Cambridge, 2004).

[59] T. Stauber, J. González, and G. Gómez-Santos, Change of chirality at magic angles of twisted bilayer graphene, Phys. Rev. B **102**, 081404(R) (2020).

[60] D. A. Bahamon, G. Gómez-Santos, D. K. Efetov, and T. Stauber, Chirality probe of twisted bilayer graphene in the linear transport regime, Nano Lett. **24**, 4478 (2024).

[61] D. Guerci, P. Simon, and C. Mora, Moiré lattice effects on the orbital magnetic response of twisted bilayer graphene and Condon instability, Phys. Rev. B **103**, 224436 (2021).

[62] M. Sánchez-Sánchez, I. Díaz, J. González, and T. Stauber, Nematic versus Kekulé phases in twisted bilayer graphene under hydrostatic pressure, arXiv:2403.03140.

[63] G. Gómez-Santos and T. Stauber, Measurable lattice effects on the charge and magnetic response in graphene, Phys. Rev. Lett. **106**, 045504 (2011).

[64] T. Stauber and H. Kohler, Quasi-flat plasmonic bands in twisted bilayer graphene, Nano Lett. **16**, 6844 (2016).